small
NANO MICRO
www.small-journal.com

Self-Powered Nanoscale Photodetectors

*Wei Tian, Yidan Wang, Liang Chen, and Liang Li**

Novel self-powered nanoscale photodetectors that can work without an external power source, which have great application potential in next-generation nanodevices that operate wirelessly and independently, are being widely studied. This review aims to give a comprehensive summary of the state-of-the-art research results on self-powered nanoscale photodetectors. An introduction of recent progress on Schottky junction photodetectors is provided. Two types of Schottky junctions are discussed in detail: metal–semiconductor and semiconductor–graphene junctions. Next, recent developments of p–n junction photodetectors are highlighted, including homojunction and heterojunction photodetectors. Then, piezo-phototronic effect enhanced photodetection performances of Schottky junctions and p–n junctions are discussed. Then, significant results on the photoelectrochemical-cell-based photodetector and integrated self-powered nanosystem are presented, followed by a systematic comparison of different types of photodetectors. Finally, a summary of the previous results is given, and the major challenges that need to be addressed in the future are outlined. The hope is that this review can provide valuable insights into the current status of self-powered photodetectors and spur new structure and device designs to further enhance photodetection performance.

1. Introduction

Recently, low-dimensional nanostructures have been intensively investigated as potential building blocks to construct optoelectronic devices.[1–10] Owing to the great advances in fabrication techniques, a large variety of semiconductor nanostructures, such as quantum dots, nanowires/rods and nanosheets, have been successfully synthesized.[11–15] This provides great opportunities to understand and exploit the fascinating features of low-dimensional materials. As a significant optoelectronic property of semiconductor nanostructures, photoresponse to light irradiation (ultraviolet (UV), visible, or infrared) is one of the mostly studied phenomena, which makes these nanostructures excellent candidates for building blocks of photodetectors.[16–25]

Nanostructures are ideal candidates for light detection, with the merits of large responsivity, a fast response speed, and an excellent detection limit.[26–28] However, until now, most nanostructure-based photosensors have been fabricated to be powered by an external power source, which is utilized to spur the photogenerated carriers to generate a photocurrent.[29–35] This remarkably increases the device size and weight. As a result, their applications in areas such as in situ medical therapy monitoring and wireless environmental sensing are seriously limited.

Constructing self-powered systems that can work independently, wirelessly, and sustainably is a significant research direction for the next-generation nanodevices and has attracted intensive research interest.[36–39] A novel self-powered photodetector that works without an external power source, which can meet the demands of a small size, reduced weight, and low power consumption for next-generation nanodevices, is being widely studied. One kind of self-driven photodetector has been designed by utilizing the photovoltaic effect.[40–62] According to the charge separation features of the interface, the current self-driven photosensors based on the photovoltaic effect can be classified into three types: Schottky junction, p–n junction, and photoelectrochemical (PEC) cell. Another kind of self-powered photodetector is constructed using an integrated nanosystem, which consists of an energy harvesting unit and a light sensor.[63–68] In such a system, the energy harvesting unit can collect energy from nature and drive the light sensor to achieve detection. This type of self-powered photodetector has been demonstrated by integration with nanogenerators, solar cells, supercapacitors, etc. The evaluation of the capabilities of photodetectors involves several important parameters: the on–off ratio, which is defined as the ratio between the photocurrent and dark current; the photoresponsivity, which is defined as the photocurrent through the detector per active area per unit power of light; and the specific detectivity, which characterizes how weak of a light the device can detect and is determined by the photoresponsivity and dark current of the photodetector. In addition, the response speed is a crucial parameter for photodetectors, which includes two values: rise time and decay time, which are defined as the times needed for the photocurrent to rise and decay, respectively, to certain values during the on and off cycles of light irradiation.[69,70]

Due to the increasingly large number of investigations that have been performed on self-powered photodetectors, a deeper understanding of the relationship of photoresponse properties with material structure and device configuration is now being achieved. Thus, a comprehensive review of self-powered

Dr. W. Tian, Y. Wang, L. Chen, Prof. L. Li
College of Physics, Optoelectronics and Energy
Collaborative Innovation Center of Suzhou Nano Science and Technology
Jiangsu Key Laboratory of Thin Films
Soochow University
Suzhou 215006, P. R. China
E-mail: lli@suda.edu.cn, liang.li0216@gmail.com

DOI: 10.1002/smll.201701848

photodetectors is necessary to summarize the great advances in this field. A systematic introduction of state-of-the-art self-powered photodetectors and a brief comparison between different types of photodetectors would facilitate the implementation of new device designs with optimized performances.

The review is organized as follows: first, we summarize the recent progress in Schottky junction photodetectors. Two types of Schottky junctions are discussed in detail: metal–semiconductor and graphene–semiconductor. Next, we highlight recent developments of p–n junction photodetectors, including homojunction and heterojunction. Then, we introduce the piezo-phototronic effect and its application in improving the photodetection performances of the Schottky junction and p–n junction. We also summarize the significant results on PEC-cell-based photodetectors, followed by the introduction of an integrated self-powered nanosystem. In the last section, future prospects in self-powered nanoscale photodetector research are provided.

Wei Tian received his Ph.D. degree from Waseda University, Japan, in 2014. Afterward he joined the National Institute for Materials Science (NIMS), Japan, as a postdoctoral researcher. Then, he joined the College of Physics, Optoelectronics and Energy, Soochow University, China, as associate professor. His research interests include the controlled fabrication and characterization of low-dimensional semiconducting nanostructures and their application in optoelectronics devices.

Liang Li received his Ph.D. degree from Institute of Solid State Physics, Chinese Academy of Sciences and won the Excellent President Scholarship in 2006. From 2007 to 2012, he worked at the National University of Singapore, Singapore, National Institute of Advanced Industrial Science and Technology & National Institute for Materials Science, Japan, and the University of Western Ontario, Canada. Since August 2012, he is a full professor in Soochow University, China. His group (http://ecs.suda.edu.cn) focuses mainly on energy conversion materials for solar cells, photodetectors, and electrochemical batteries. His publications have generated over 6000 citations. He currently has an H-index 40.

2. Schottky-Junction-Based Photodetectors

The device configuration of photodetectors is crucial for their photodetection capability. The conventional design of nanoscale photodetectors usually incorporates a semiconductor with two Ohmic metal contacts. An external bias is required to separate the photogenerated electron–hole pairs. Ohmic contact photodetectors normally possess excellent properties such as large photoconductive gain and high responsivity.[20–23] If one of the two Ohmic contact ends is replaced by a Schottky barrier contact, nonsymmetrical Schottky contact devices can be obtained. Unlike Ohmic contact devices, Schottky junction photodetectors are sensitive and have fast response speeds. More importantly, Schottky junction photodetectors rely on the presence of a built-in potential in a junction to achieve the separation and transport of the photogenerated carriers, which renders them capable of detecting light illumination without an external bias voltage.[71–75]

2.1. Semiconductor–Metal Schottky Junction

Because of the different work functions and band alignments between a semiconductor and a metal, a Schottky junction is generally formed at their interface.[71] A Schottky junction can be utilized to construct highly sensitive and fast-responsive nanowire sensors to detect biomolecules, gases, and UV light, which has been demonstrated by Wang and co-workers.[72–75] For example, a ZnO-based photosensor exhibited greatly enhanced UV sensitivity (an enhancement of 10^4 times) and its decay time was remarkably shortened from 417 to 0.8 s when a Schottky contact was utilized in device fabrication instead of an Ohmic contact.[72] Moreover, upon illumination, the built-in potential at the interface of the Schottky junction drove the photoexcited holes and electrons to move in opposite directions, forming an electric current. In other words, the Schottky-junction-based photosensors can achieve light detection without external power sources. In 2010, Zhang et al. fabricated a self-driven UV photodetector from an individual Sb-doped ZnO nanobelt/Au Schottky contact (**Figure 1**a).[43] Without an external bias voltage, the fabricated device exhibited a high sensitivity and a fast response to UV light. In the dark, an obvious rectifying behavior was observed in the current–voltage (I–V) curve of the device. Upon illumination by a UV laser of the ZnO/Au junction, the device exhibited an almost-linear I–V curve. At zero bias, the on–off ratio of the fabricated device was as high as 22, and the response time was less than 100 ms. It is worth noting that no obvious change was observed in the I–V curves when the UV laser was focused on the nanobelt instead of the Schottky junction, which suggests that the Schottky contact dominated the photoresponse of the photodetector without a bias voltage. When UV light illuminated the junction, the recombination rate in this field was significantly reduced. As shown in Figure 1b, the Schottky-junction-induced localized electric field separated the photoexcited electrons and holes in this area and drove them to move in opposite directions, thus leading to a large photocurrent.

Enlightened by the above work, Luo and co-workers successfully fabricated a Ga-doped CdS nanoribbon/Au Schottky-junction-based self-driven photodetector.[47] In the

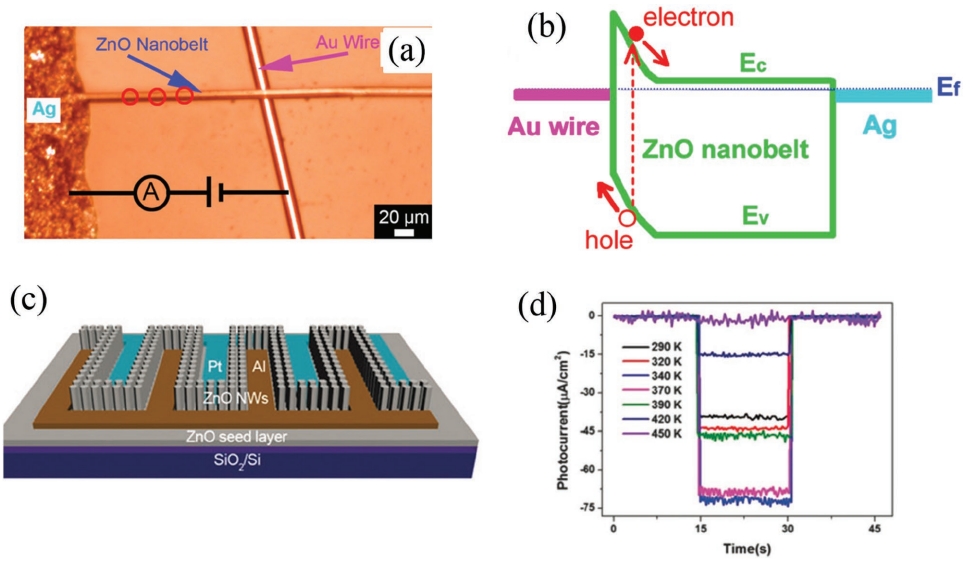

Figure 1. a) Optical image of the photodetector based on the Au–ZnO nanobelt Schottky junction. b) Schematic band diagram of the junction under UV light illumination. Reproduced with permission.[43] Copyright 2010, American Institute of Physics. c) Schematic diagram of the photodetector based on ZnO nanowire arrays and the Pt Schottky contact. d) Photocurrent as a function of time for the self-driven photodetector, tested at different temperatures at zero bias. Reproduced with permission.[45] Copyright 2014, The Royal Society of Chemistry.

dark, a rectification ratio of 10^6 within ±1 V was achieved for the device. Under light illumination, the device exhibited obvious photovoltaic behavior. Optoelectronics results revealed its high sensitivity to light irradiation as well as excellent reproducibility and stability. Particularly for CdS:Ga (8%) nanoribbons/Au, high responsivity (8 A W^{-1}) and greater-than-unity photoconductive gain (20) were attained. Fast response speeds (rise and decay times of 95 and 290 μs) were also achieved for this device.

The above two investigations focused on the utilization of a single nanostructure to construct a Schottky junction with metal. However, the contact area of a single nanostructure with metal electrodes is very small, resulting in a very weak response current. In addition, single-nanowire-based Schottky junctions usually require complex fabrication processes. Alternatively, nanowire arrays coupled with metallic contacts open up a novel platform to assemble individual nanowires into large-area optoelectronic devices. For instance, Bai et al. demonstrated the fabrication of a self-powered UV photodetector from ZnO nanowire arrays selectively grown in the gaps between the fingers of the Al–Pt interdigitated electrodes (Figure 1c).[45] Under the illumination of a 355 nm laser (23 mW cm^{-2}), the device exhibited an obvious photoresponse with an on–off ratio of 1.7×10^4 without an external power supply. The rise time and recovery time were 81 and 95 ms, respectively, which are much faster than those of ZnO-nanowire-array-based photoconductive photosensors.[76] This can be attributed to the different photoresponse mechanisms. For the conventional ZnO-based photoconductive photodetector, the photoresponse is related to the oxygen adsorption and desorption process on the nanowire surface, resulting in a long-time photoelectrical response. For the Schottky type detector, a strong built-in electric field is created because of the Pt Schottky contacts. Driven by the internal potential, the photogenerated electrons and holes flow toward the n-ZnO side and Pt side, respectively, leading to a large photocurrent at zero bias. Thus, the drifting of the majority carriers in the depletion zone and the diffusion of the minority carriers outside the space charge region dominate the photoresponse speed. This is distinct from the long-time photoelectrical response of the ZnO photoconductive photodetector.[77]

The authors also investigated the effect of temperature on the detection characteristics of the device at zero bias. The device photoresponse at zero bias showed an obvious dependence on the temperature (Figure 1d). At a certain light power intensity, the sensitivity increased first and then decreased with the increase of temperature. According to the thermionic emission–diffusion theory, the change in the difference between the Schottky barrier height (△SBH) at the two ends of the device as a function of temperature was drawn. It was clearly observed that △SBH had the same trend as the photocurrent with the increase of temperature, indicating that the Schottky barrier dominated the photoresponse of the photodetector under zero bias. The device achieved an ultrahigh sensitivity of 3.1×10^4 at 340 K at zero bias, which represents an 82% enhancement compared to that at room temperature. This work demonstrated that heating is an effective method to modulate the performance of a self-powered photodetector.

In recent years, Schottky-type self-driven photodetectors have been extensively studied. Apart from the abovementioned ZnO and CdS, researchers have built a large variety of material systems for Schottky-type self-powered photodetectors. For example, PbS quantum dots prepared via halogen–ligand exchange were contacted with indium (In) to create Schottky barrier diodes, which can act as high-performance visible-near-infrared photodetectors at zero bias voltage.[41] A self-powered solar-blind photodetector with a fast response was fabricated based on a β-Ga_2O_3 nanowire array/Au Schottky junction.[42] In addition, novel device structures were developed to further

enhance the photodetection ability of Schottky junction photodetectors. For instance, He et al. fabricated a novel kind of self-powered photodetector that included two opposite Schottky junctions, which were formed by one layer of Au nanoparticles sandwiched between two layers of TiO_2 nanorods.[78] The device can perform independently and is powered only by the two opposite Schottky junctions without an external power supply. Due to the rationally designed structure, the device exhibited a high photoresponsivity of ≈1.0 A W^{-1} to UV light, with a fast response speed (rise and decay times of 0.33 and 0.6 s, respectively) at zero bias.

2.2. Semiconductor–Graphene Schottky Junction

Schottky junctions have many merits, such as easy fabrication processes and material universality. Unfortunately, the strong light absorption of metals may severely restrict the capability of the Schottky-junction-based photosensors. As an excellent candidate for a transparent electrode, graphene has fascinating properties, including high optical transmittance, large electrical conductivity, and a tunable work function.[79] Because of these outstanding features, various semiconductor materials, including ZnO, CdSe, and Ge, have been integrated with graphene to form Schottky junctions to achieve self-driven light detection.[48,53,80] For example, Dai et al. applied graphene as a replacement for metal and designed a self-driven CdSe nanobelt/graphene Schottky junction photodetector (**Figure 2**a).[53] Without an external bias voltage, the device showed a high sensitivity (3.5×10^5). In a broad range of switching frequencies up to 1000 Hz, the device achieved a fast response speed (rise and decay times of 82 and 179 ms, respectively) (Figure 2b). The photoresponsivity was measured as 10.2 A W^{-1} and photoconductive gain as ≈28. The energy band diagram was illustrated to gain insight into the working mechanism of the self-powered photodetector (Figure 2c). Because of the work function difference between graphene (4.6 eV) and CdSe (4.2 eV), a built-in electric field is created between them. Under irradiation by light with above-band-gap energy, the photoexcited holes and electrons are driven toward the CdSe nanobelt and graphene, respectively, by the built-in field, leading to a short-circuit current.

As a typical material of group IV, Ge possesses a large absorption coefficient at near-infrared frequency.[81] Thus, the integration of Ge with graphene can achieve infrared light detection. Recently, Luo et al. successfully combined graphene with a bulk Ge wafer to form a Schottky junction diode, which can work at zero bias.[48] The photoresponsivity, detectivity, and response time of the device were calculated to be 51.8 mA W^{-1}, 1.38×10^{10} Jones, and 23 μs, respectively. Meanwhile, the device exhibited evident spectral selectivity with the highest sensitivity at 1400 nm, suggesting its potential application for infrared detection.

Owing to the Schottky contact configuration, the photodetection characteristics of the Schottky-junction-based photodetector are remarkably influenced by the quality of the interface between the semiconductor and graphene. For example, there are a large number of surface states that pin the surface Fermi level at the interface between graphene and Si, resulting in strong leakage current noise, which degrades the capability of graphene/Si Schottky-based devices. Consequently, graphene/Si photodiodes suffer from an inferior on–off ratio, low responsivity and low specific detectivity.[82,83] To improve these parameters, interface modification is a promising approach. Through in situ surface decoration of a MoO_3 overlayer on graphene, Chen et al. demonstrated a notable performance improvement of a graphene/Si self-powered photodetector.[50] The photoresponsivity of the MoO_3-doped graphene/Si device was greatly enhanced under a broad wavelength range from UV to near infrared, with a maximum value of 0.4 A W^{-1} at 750 nm light illumination. The introduction of the MoO_3 layer also boosted the specific detectivity to 5.4×10^{12} Jones in the wavelength range from 600 to 800 nm. The authors ascribed the remarkable performance improvement to the reduced series resistance of the device and increased SBH at the graphene/Si interface after MoO_3 functionalization, which were beneficial for the photocarrier separation and collection processes. Later, Li et al. reported a graphene/Si Schottky junction with further enhanced performance through the insertion of an interfacial oxide layer between graphene and Si (Figure 2d).[51] After introducing a thin interfacial oxide layer, the dark current of the graphene/Si heterojunction at zero bias was remarkably reduced by two orders of magnitude (Figure 2e). The device with interfacial oxide possessed a specific detectivity of up to 5.77×10^{13} Jones in vacuum. This was the highest reported value for planar graphene/Si photodetectors at room temperature. Moreover, the improved graphene/Si Schottky junction photodetectors exhibited a high responsivity of 0.73 A W^{-1} and a high on–off ratio of up to 10^7. As shown in the energy-band diagram (Figure 2f), the thin oxide layer between graphene and Si acts as a blocking layer, which can effectively depress the dark current of the junction. Thus, large on–off current ratio and specific detectivity were achieved after the introduction of the thin oxide layer. These results demonstrated that the interface modification of the graphene/Si Schottky junction was a promising approach to the construction of high-performance self-powered photodetectors. Apart from the above methods, other approaches have been introduced to improve the photodetection performances of Schottky-junction-based photodetectors, which will be discussed in Section 4.

In this section, two types of Schottky junction are discussed in detail: semiconductor–metal and semiconductor–graphene. A diverse range of material systems for Schottky-type self-powered photodetectors have been demonstrated, and exciting results have been obtained. Particularly for the semiconductor–graphene junction, self-powered photodetectors with outstanding performances were developed by integrating various semiconductor materials with graphene. Further performance enhancement was achieved by interface engineering.

3. p–n-Junction-Based Photodetectors

As fundamental components of optoelectronic devices, p–n junctions play a crucial role in modern microelectronics applications and have been widely applied to the fabrication of conventional photodetectors based on bulk films.[84,85] In the past decade, the concepts and architectures (p–n and p–i–n

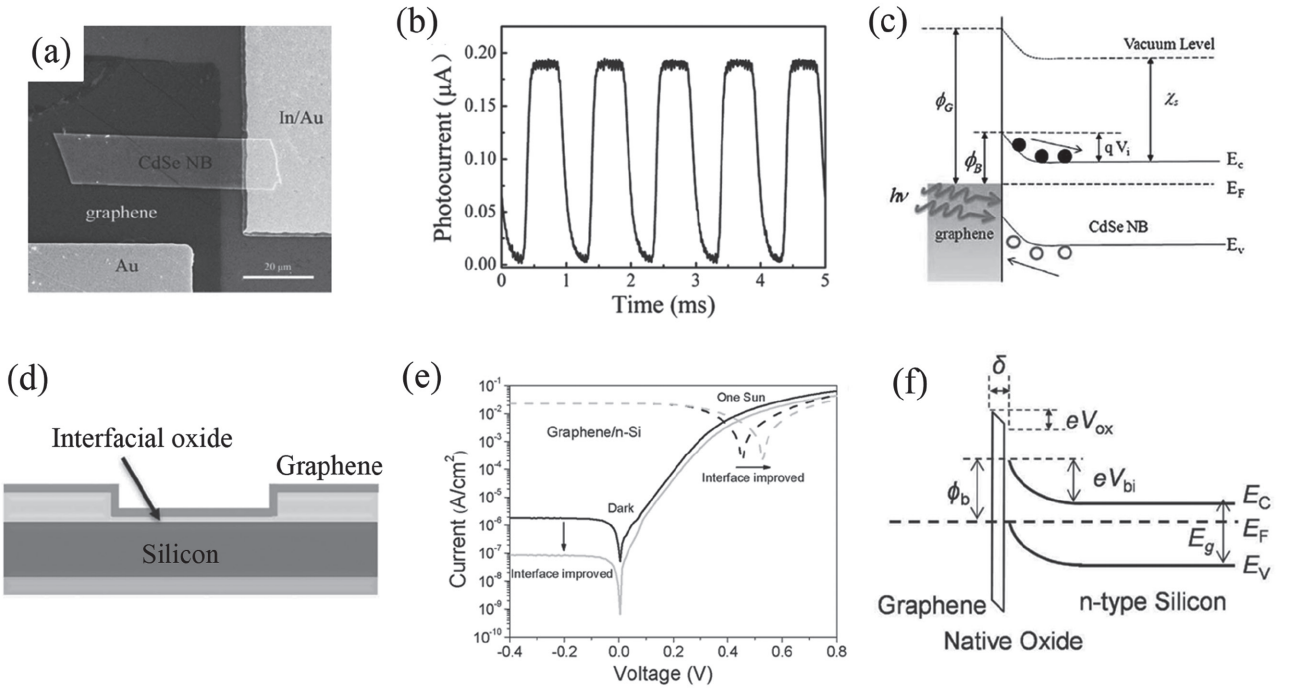

Figure 2. a) A scanning electron microscopy (SEM) image of the CdSe nanobelt/graphene Schottky-junction-based photodetector. b) Photocurrent response of the device under a light switching frequency of 1000 Hz. c) The energy band diagrams of the device under light illumination. E_C, E_V, and E_F represent the conduction band edge, valence band edge, and Fermi level, respectively. Reproduced with permission.[53] Copyright 2012, The Royal Society of Chemistry. d) A schematic illustration of a graphene/Si junction with interfacial modification. e) The current–voltage curves of the as-fabricated device with or without 2 nm thick interfacial modification. f) The energy-band diagram of a graphene/Si junction with interfacial modification. Reproduced with permission.[51] Copyright 2016, Wiley-VCH.

junctions) in conventional photodetectors have been replicated in nanostructures. Nanostructured p–n junctions with various configurations, such as core–shell, axial, crossed, and branched structures, have been fabricated to construct self-powered nanoscale photodetectors. Moreover, the possibility to transfer or directly grow nanostructures (single nanowires, nanowire arrays, or 2D nanomaterials) on substrates largely enriches the material combinations and device architectures.[86]

3.1. p–n Homojunction

Among semiconductor nanostructures, Si nanowires are regarded as a significant class of nanoscale components for highly efficient optoelectronic devices because of their fascinating optical and physical properties.[87] Benefiting from sophisticated techniques such as chemical vapor deposition (CVD) and the ion etching method, Si nanowires with p-/n-type conductivity can be easily produced, which allow for the construction of Si-nanowire-based p–n homojunctions.[88–90] As a pioneering work, Lieber and co-workers in 2007 reported the successful fabrication of individual p-type/intrinsic/n-type (p–i–n) coaxial Si homojunction nanowires and demonstrated their photovoltaic properties as solar cells.[91] Since then, tremendous efforts have been made to fabricate various p–n homojunction nanostructures, such as axial or radial single-nanowire homojunctions, vertical nanowire array homojunctions (a p/n-type nanowire array on an n/p-type film), and vertical core/shell nanowire array homojunctions (a p–n junction nanowire array on a transparent conductive oxide substrate).[57,92–95] The application of p–n homojunctions in solar power conversion devices has achieved tremendous advances. Due to the limited space, we will only review in more detail the p–n homojunction structures used for self-powered photodetection.

The current investigations of p–n homojunctions are mainly focused on Si, ZnO, and several group III–V compound semiconductors. Among them, ZnO p–n junctions are the most intensively studied materials in photodetectors due to their suitable bandgap and facile fabrication.[96] As an example, Wang et al. reported a ZnO p–n homojunction based on Sb-doped p-type ZnO nanowire arrays grown by CVD on n-type ZnO films on sapphire substrates.[97] The homojunction exhibited an obvious rectification characteristic with a turn-on voltage of ≈3 V. The photocurrent measurements revealed that the device showed very good response to UV light illumination. The response spectrum extended from 280 nm and steadily increased up to 380 nm (3.26 eV), which corresponds to the band gap of ZnO. All these results demonstrated that a homojunction self-powered UV photodetector can be obtained on the basis of a p-type nanowire array and an n-type thin film.

ZnO axial single-nanowire homojunctions can also be applied to build self-powered photodetectors. Cho et al. reported a p–n homojunction ZnO nanowire fabricated with in situ arsenic doping to obtain a p-type segment continuously on top of the as-grown n-type segment.[98] The p–n homojunction can work in a self-powered mode. The device exhibited a large on–off

ratio of 10^6 at zero bias voltage as well as stable and repetitive responses under light on and off cycles. After switching off the UV light, the photocurrent quickly returned to the initial levels of the dark current. Its rise time (30 ms) and decay time (50 ms) are much smaller than those of previously reported photoconductive ZnO UV detectors. The working mechanism of the p–n homojunction photodetectors is described as follows. p-ZnO possesses a low density of electrons and is rich in holes, while n-ZnO has a high concentration of electrons but few holes. When p-ZnO and n-ZnO form a junction, carrier diffusion occurs at the interface owing to the high carrier concentration gradient at the junction. As a consequence, electrons diffuse from the n-type side to the p-type side, while holes diffuse in the opposite direction. However, the donors and acceptors are fixed in space. When holes diffuse from the p-ZnO side to the n-ZnO side, they leave behind uncompensated acceptors in the p-type region, and electrons leaving the n-ZnO part create uncompensated donors. The diffusion of electrons and holes from the vicinity of the junction establishes a region of positive space charge near the n-type side and negative charge near the p-type side. An electric field is built up at the interface. Upon illumination, the photoexcited electron–hole pairs can be efficiently separated by the built-in electric field. As a result, the holes move to the valence band of the p-type ZnO, while electrons flow to the conduction band of the n-type ZnO, leading to a short-circuit current.

In addition to 1D nanostructures, 2D semiconductors based on p–n homojunctions have attracted tremendous attention for their versatility in applications due to their promising electrical, optical, and mechanical properties.[15] Recently, Ang et al. reported a facile spatially controlled Al-doping strategy that enables the realization of a p–n homojunction photodiode within a few-layer black phosphorus (BP) nanosheet.[16] High near-infrared photovoltaic performance, with an open-circuit voltage responsivity of 15.7×10^3 V W^{-1} and a short-circuit current responsivity of 6.2 mA W^{-1} at room temperature, was achieved for this device, as the built-in electric field at the p–n homojunction interface efficiently separated the photogenerated electron–hole pairs without any external bias.

3.2. p–n Heterojunction

Despite the great progress achieved in the past, employing p–n homojunctions as building blocks to construct high-performance self-powered photodetectors remains a big challenge. A doping technique is usually used to fabricate the homojunction, requiring strict experimental conditions and a complex fabrication process, which inevitably bring high cost. In addition, except for Si, ZnO, and several group III–V compound semiconductors, reproducible and reliable p-type nanomaterials are still not available because of several factors, such as low solubility of dopants, deep acceptor levels, and a self-compensation process.[99] Additionally, owing to the narrow light absorption region, p–n homojunction-based photodetectors generally suffer from weak absorption of incident light, which significantly limits the improvement of their device parameters. In contrast, p–n heterojunctions can achieve enhanced light absorption and possess larger absorption ranges owing to the presence of two or more materials with different bandgaps in the heterojunctions, which greatly improves the device performance and broadens the response spectrum.

In 2011, Yu et al. constructed a heterojunction based on an individual n-type ZnO nanowire and a p-type GaN film (**Figure 3**a) and demonstrated its utilization as a self-driven visible-blind UV detector that gives a photocurrent response of 2 μA under 325 nm laser irradiation (Figure 3b).[100] A fast response speed, with rise and decay times of 20 and 219 μs, was achieved for this device. Powered by the photovoltaic effect of the ZnO/GaN p–n heterojunction, the device exhibited a short-circuit current density of up to 5×10^4 mA cm^{-2}, an open-circuit voltage of 2.7 V, and a maximum output power of 1.1 μW.

Inspired by the above work, tremendous research efforts have been devoted to fabricating ZnO-based p–n photodiodes. One seminal work was reported by Dunn et al. They employed an n-type ZnO nanorod array and a p-type copper thiocyanate (CuSCN) film to form a p–n heterojunction (Figure 3c).[101] The device performed well as a UV detector that operates without an external power source, with a distinct photocurrent of 4.5 μA under UV illumination of 6.0 mW cm^{-2}. A UV–visible rejection ratio of 10^2 was obtained with fast rise and decay times (500 ns and 6.7 μs). Interestingly, it was observed that the photocurrent under a forward bias alternated between positive and negative when the UV light was switched on and off. As shown in Figure 3d, the device demonstrated a photovoltaic effect under UV light illumination at zero bias and a small photocurrent under a forward bias. This feature enabled the device to realize an on–off binary photoresponse to UV light. At a small forward bias (0.1 mV), the device showed an ultrafast response speed with a rise time of 4 ns, which exceeded those of both Schottky and p–n junction ZnO-based photodetectors in previous works. The binary response of the current device arose from the low turn-on voltage (≈0 V) of the diode and the photovoltaic behavior, as confirmed in the typical *I*–*V* plot of the device. The authors ascribed this to the well-aligned band structures of FTO, ZnO, CuSCN, and Au. Their electron affinities and Fermi levels are closely coordinated. This allows fast charge-carrier separation at the interface, preventing photogenerated electrons in ZnO from recombining with holes at the p–n junction. One additional advantage of this p–n diode was its excellent stability. Surprisingly, after storage in ambient conditions over six months, there was no obvious degradation of the performance. This can be attributed to the impregnation of p-type CuSCN into the ZnO nanostructure, which effectively prevented the degradation of the device.

The rational design of the material morphology in the p–n junction to strengthen the light absorption efficiency and improve interfacial charge dynamics is crucial for obtaining high photodetection performance. Fang et al. reported a novel heterojunction structure built from p-type NiO mesoporous nanosheets and n-type TiO_2 nanowells.[17] In this structure, a thin layer of TiO_2 nanowells enables faster charge carrier transport through a shorter diffusion pathway along the lateral direction, and the flower-like NiO nanosheets guarantee the exposure of the interfacial active reaction sites to UV light, which takes great advantage of the p–n junction area to enhance the generation of electron–hole pairs. As a result, this p–n junction

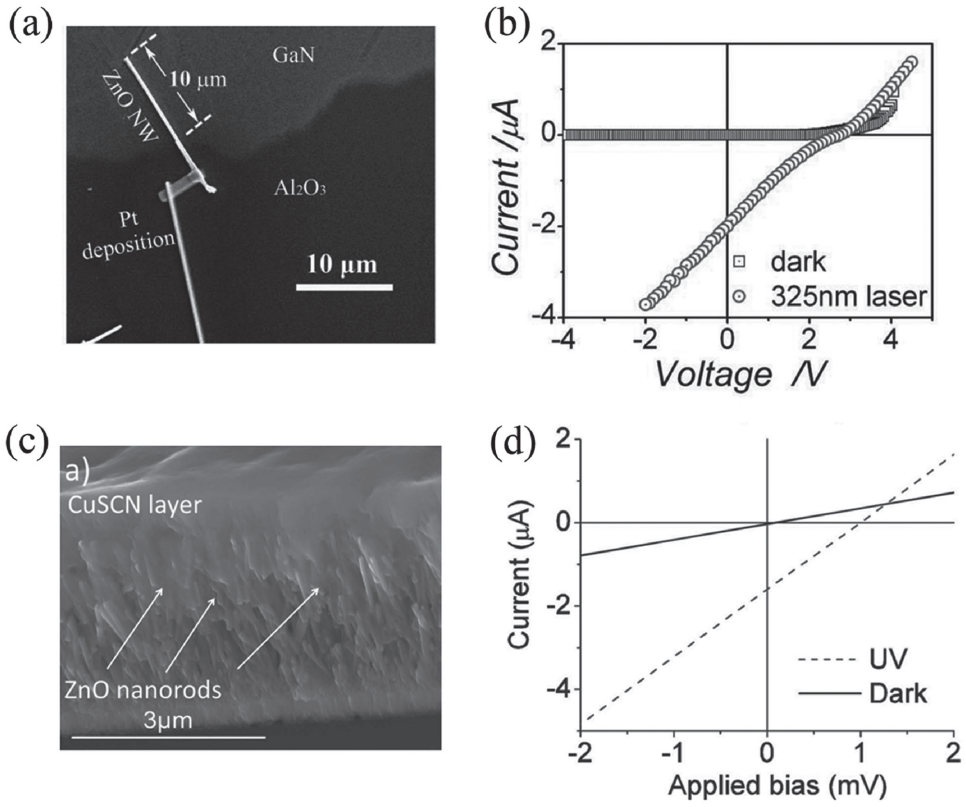

Figure 3. a) SEM image of the ZnO nanowire/GaN film junction. b) *I–V* curves of the p–n junction in the dark and under UV illumination. Reproduced with permission.[100] Copyright 2011, Wiley-VCH. c) Cross-sectional SEM image of the ZnO–CuSCN p–n junction. d) Typical *I–V* curves for the device under darkness and UV illumination. Reproduced with permission.[101] Copyright 2013, Wiley-VCH.

photodetector yielded a responsivity of as high as 42 μA W^{-1} under 350 nm light illumination at 0 V bias, which corresponds to a detectivity of 1.1×10^9 Jones. The mechanism of the self-powered device can be understood on the basis of the energy band structure. Once in contact, a depletion region is created at the n-type TiO_2/p-type NiO interface because of carrier diffusion under thermal equilibrium conditions, which gives rise to a built-in electric field and provides a driving force for the charge separation. Upon above-bandgap light irradiation, the built-in electric field inside the depletion region efficiently separates the photoexcited electron–hole pairs. As a result, the holes move to the valence band of the p-type NiO, while electrons flow to the conduction band of the n-type TiO_2, resulting in a photovoltaic current in the external circuit. Moreover, the minority carriers produced within the diffusion length from the depletion region can also diffuse to the depletion region and be extracted by the built-in electric field. The photovoltage is a result of the energy difference between the Fermi levels of NiO and TiO_2 under illumination. This photovoltaic effect enables the p–n junction to detect UV light without an external bias. Recently, Fan et al. fabricated a high-quality γ-In_2S_{e3}/Si heterojunction photodiode.[58] The direct and narrow bandgap, as well as the high absorption coefficient of γ-In_2Se_3, is beneficial for light harvesting and the generation of electron–hole pairs. In addition, the strong built-in electric field near the γ-In_2Se_3/Si interface benefited from the flowerlike morphology of γ-In_2Se_3 with a high surface area, resulting in enhanced photoelectrical performance. Accordingly, an efficient heterojunction photodiode was achieved, which possessed remarkable responsivity (5.67 A W^{-1}) and detectivity (5.66×10^{13} Jones) over a wide range of wavelengths at zero bias.

Because of the nanowire array geometry, core–shell p–n junction nanowire arrays have several particular advantages for self-powered photodetector applications.[102] First, due to its geometry, a nanowire array possesses excellent light harvesting ability. Particularly for heterojunctions, more light can be absorbed because the absorption edge is determined by the lower bandgap material. Second, such radial junction architecture provides reduced travel distances of photogenerated minority carriers to the collective electrodes, resulting in reduced bulk recombination and improved carrier collection efficiency. Thus, a high photocurrent can be achieved. Third, owing to the highly developed scalable approaches, including CVD, MBE, and the hydrothermal method, it is easy to fabricate vertically aligned nanowire arrays over large areas on different substrates.[103,104] The above merits make radial p–n junctions (core–shell nanowires) highly promising for self-powered photodetector applications.

In one of the earliest studies on core–shell heterojunction-based self-powered photodetectors, Ray and co-workers reported the fabrication and photoresponse properties of p-Ge/n-CdS core–shell nanowire radial heterojunctions, which were synthesized by growing CdS nanoparticles on Ge nanowires (**Figure 4**a).[105] Although they did not show

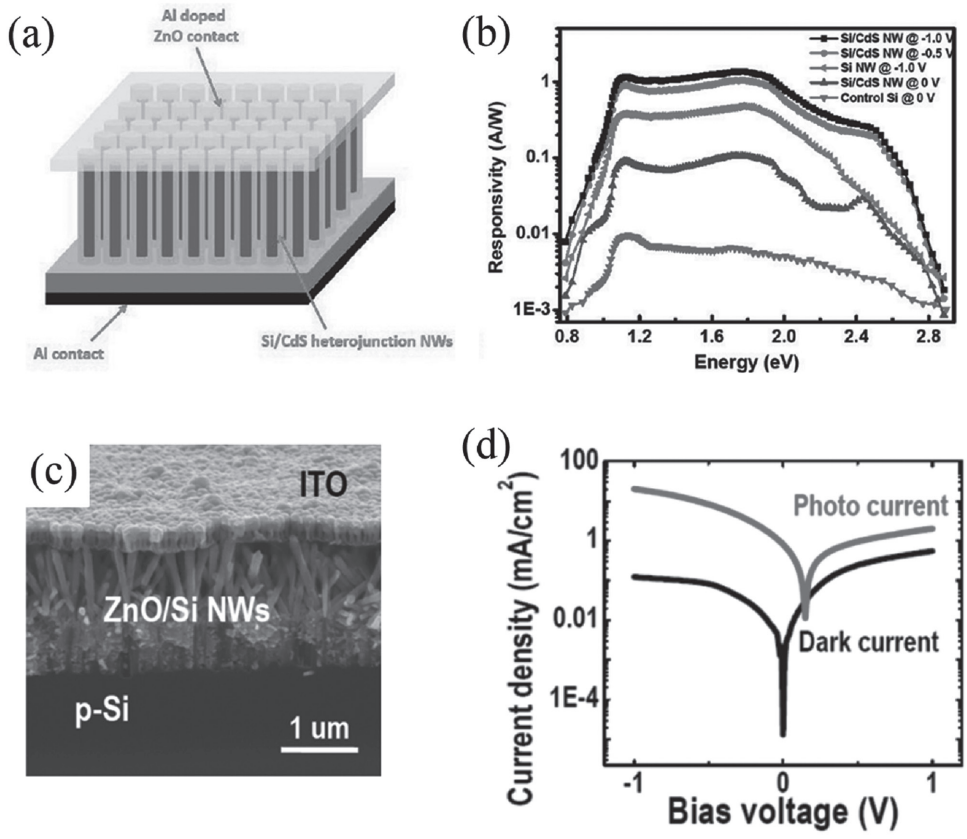

Figure 4. a) Schematic illustration of the Si/CdS core–shell heterojunction device. b) The comparative spectral responsivity curves of planar Si, Si nanowires, and Si/CdS core/shell nanowire photosensors. Reproduced with permission.[106] Copyright 2012, American Chemical Society. c) SEM image of the ZnO/Si branched heterojunction-based photodetector. d) *I–V* characteristics measured in the dark and under xenon lamp illumination. Reproduced with permission.[113] Copyright 2010, American Chemical Society.

the photoresponse results of the heterojunction at zero bias, the diode-like behavior observed in the *I–V* curves indicated the self-powered functionality of the photodetector. Interestingly, the heterojunction showed an enhanced wide photoresponse, ranging from 450 to 1000 nm (Figure 4b), which was beyond the response region of bulk Ge. This can be ascribed to the existence of sub-band defects near the junctions and the quantum confinement effect in Ge nanowires. Later, the same group constructed highly efficient self-powered photodetectors based on Si/CdS radial nanowire heterojunctions.[106] The dark and photocurrent densities of the device were measured to be 1.0×10^{-6} and 2.11×10^{-5} A cm^{-2} under zero bias, giving rise to an on–off ratio of 21.1. The maximum spectral responsivity of 0.11 A W^{-1} was attained at a wavelength of 700 nm. The responsivity was remarkably improved when the reverse bias voltage was further increased. The peak values of responsivity were boosted to 1.05 and 1.37 A W^{-1} at biases of –0.5 and –1 V, respectively. Furthermore, a broadband response ranging from 0.8 to 3.1 eV was achieved for the core–shell Si/CdS nanowires. In comparison with the control samples (radial p-Si and Si nanowires), the core–shell heterojunction exhibited enhanced performance in terms of photocurrent and responsivity under the same test conditions. All these results suggested that the radial heterojunction is suitable for constructing photodetectors with large responsivity and a wide spectral range.

Enlightened by the above works, a large variety of core–shell nanowire heterojunctions have been fabricated. Since the fabrication of ZnO and Si nanowires is facile and reproducible, various semiconductors have been combined with them to form core–shell heterojunctions, such as carbon quantum dots/Si, ZnO/CuS, and ZnO/NiO.[57,95,107–109] Because of the efficient separation of photoexcited holes and electrons in the depletion layer, driven by a built-in field for the radial heterojunctions, impressive photodetection performances have been achieved for these materials.

Apart from the core–shell structures, branched nanostructures made of a primary nanowire backbone and a secondary nanowire branch in a tree-like structure have attracted much interest due to their excellent properties relative to those of their single components.[110–112] By rationally controlling the compositions of the backbone and branch nanowires during the synthesis process, p–n heterojunctions with unique electronic and optoelectronic properties can be obtained. Moreover, branched heterostructures provide remarkably increased surface area and improved functionality and are thus very promising for utilization in electronic devices. For example, Wang et al. reported the production of n-ZnO/p-Si branched nanowire heterojunction photodiodes through a facile solution-phase process (Figure 4c).[113] Si nanowire arrays were synthesized using a metal-assisted chemical etching process,

followed by the growth of ZnO nanorods on the Si nanowire backbone with a hydrothermal process. Figure 4d shows the *I–V* curves, which were measured in darkness and under xenon lamp illumination. The ZnO/Si branched heterojunction showed a broad photoresponse, ranging from 400 to 1100 nm, with a peak responsivity of 12.8 mA W^{-1} at ≈900 nm and a maximum quantum efficiency of 2.20%. These results demonstrated that the strong light trapping of branched nanowire arrays, resulting from the high-refractive-index material filling, and the aperiodically arranged nanowire array were conducive to broadband photon detection.

The aforementioned p–n junctions are mainly based on inorganic nanostructured materials, which possess unique characteristics such as a high absorption coefficient and large carrier mobility. However, they still suffer from several shortcomings, including a high-temperature fabrication process, complicated integration steps and inferior flexibility. In contrast, organic semiconductors are solution processable, with superior flexibility and functional tenability through monomeric/molecular modifications. Unfortunately, they usually possess low carrier mobility values.[114] Accordingly, it is expected that the above drawbacks will be overcome by designing hybrid organic–inorganic p–n junctions, which have been demonstrated as building blocks in the construction of high-performance self-powered photodetectors.

One of the earliest studies on hybrid organic–inorganic p–n junction-based photodetectors was reported by Liu et al. They constructed a blue-light photosensor using polyaniline (PANI)/CdS p–n heterojunction nanowire arrays as active materials (**Figure 5**a).[115] The device exhibited light-controlled diode performance as well as evident rectifying features, although the authors did not study the self-bias performance of this device. In addition, the device exhibited a sensitive spectral response to blue light (420 nm) with a fast response speed. The straight-line behavior observed for the rectification ratio as a function of various light intensities implied that the device can achieve quantitative detection. Since then, much effort has been devoted to fabricating various hybrid inorganic–organic heterojunctions and studying their self-powered photodetection performance. For example, Game et al. prepared a self-driven UV photodetector based on n-type ZnO nanorod arrays and p-type 2,2′,7,7′-tetrakis-(N,N-di-p-methoxyphenyl-amine)-9,9′-spirobifluorene (Spiro-MeOTAD) (Figure 5b).[116] The device showed a large photocurrent density with a distinct UV–vis rejection ratio (10^2). Its photoresponsivity was ≈2.5 times higher than that of the abovementioned all-inorganic CuSCN–ZnO p–n junction.[101] The device showed a fast photoresponse speed (a rise time of 200 μs and a decay time of 950 μs). Furthermore, an efficient self-driven visible-light photosensor can be realized by simply doping the ZnO nanorod. The responsivity extended into the visible region up to 650 nm with a peak responsivity of 6.5 mA W^{-1} at 470 nm after nitrogen incorporation into the ZnO nanorod array. Another interesting work, which was reported by Fang et al., concerns a heterojunction that consists of n-type TiO_2 nanowells and p-type PANI (Figure 5c).[117] In this structure, ordered TiO_2 nanowell arrays acted as pathways for electron transport and light-scattering nanostructures, and PANI served as the hole transport layer. As a result, a highly efficient self-powered photodetector with a high on–off ratio, a fast response speed and excellent stability was obtained. The aforementioned organic–inorganic p–n junctions are all based on rigid substrates, which restricts their application in some harsh conditions. Recently, Zeng and co-workers reported a self-powered fiber-shaped wearable omnidirectional UV photodetector.[118] First, the ZnO nanowire arrays were uniformly grown on a Zn wire with high crystallinity, and the poly(N-vinylcarbazole) (PVK) and poly(3,4-ethylenedioxythiophene):poly(styrenesulfonate) (PEDOT:PSS) layers were in tight contact with ZnO. Then, the sample was twisted with carbon nanotube fiber as one electrode and the exposed Zn wire as the other electrode. The device exhibited an on–off ratio of 2 under zero bias, with a responsivity of 9.96 mA W^{-1} at 350 nm. In addition, the device could stably operate under different bending states. The authors ascribed the self-powered property to the p–n heterojunction between the ZnO and PVK layers.

Emerging as a new class of artificial nanomaterials with fascinating physical properties, van der Waals (vdW) heterostructures can be achieved by integrating different 2D crystals. A large variety of 2D vdW heterostructures have already been employed to create high-performance photovoltaic cells, field effect transistors, barristors, inverters, and memory devices.[119–121] 2D layered-material-based heterostructures possess several unique advantages for applications in photodetectors. First, their atomically thin thickness results in shortened charge transport time and distance, which are beneficial for the response speed and responsivity. Second, an intrinsic surface free of dangling bonds and weak vdW interactions enables 2D layered materials to create high-quality heterojunctions without the constraints of lattice mismatch. Last, strong light–matter interactions lead to enhanced light absorption and electron–hole pair generation, which are beneficial for building

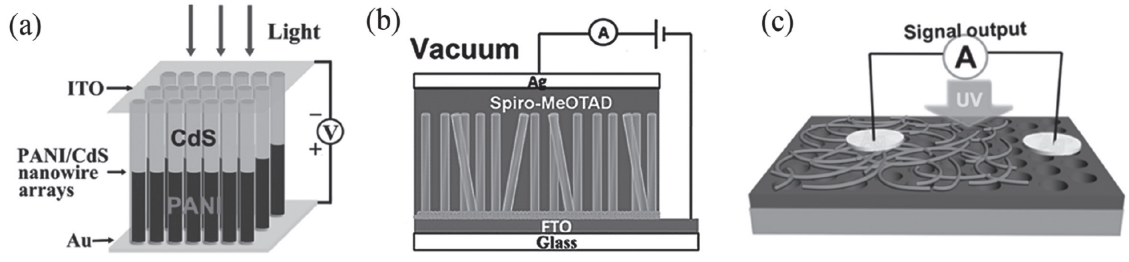

Figure 5. Device schematics of a) the PANI/CdS heterojunction nanowire array device, b) the ZnO nanorod array-Spiro-MeOTAD heterojunction device, and c) the TiO_2 nanowell-PANI heterojunction device. a) Reproduced with permission.[115] Copyright 2011, American Chemical Society. b) Reproduced with permission.[116] Copyright 2014, The Royal Society of Chemistry. c) Reproduced with permission.[117] Copyright 2016, American Chemical Society.

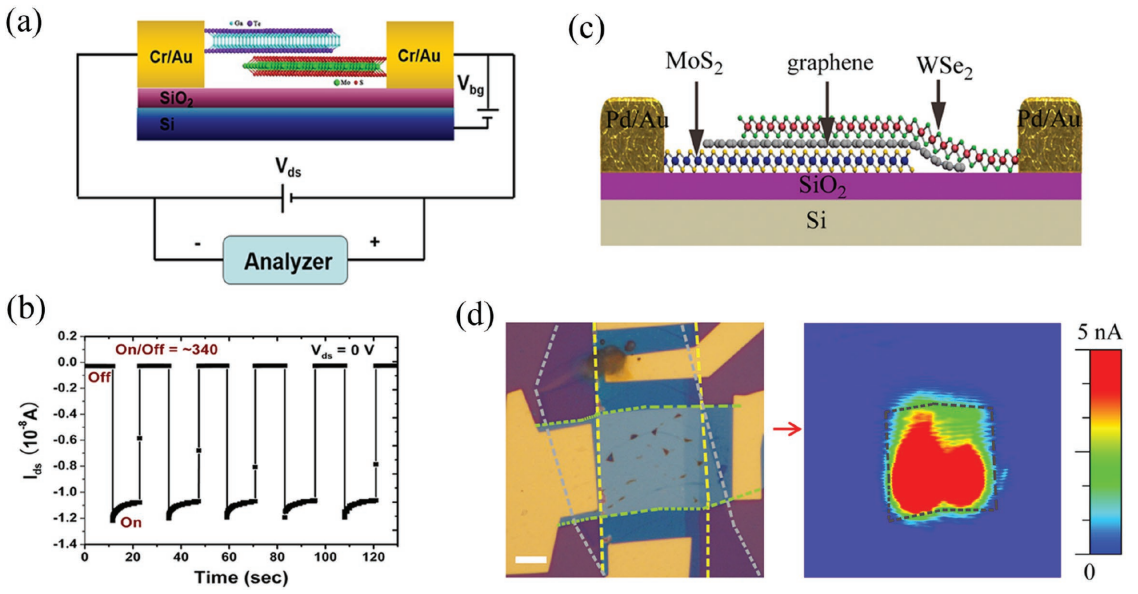

Figure 6. a) Schematic diagram of the GaTe–MoS_2 heterostructure transistors. b) Photoswitch behavior of the heterostructure photodetector at V_{ds} = 0 V. Reproduced with permission.[122] Copyright 2016, American Chemical Society. c) Schematic diagram of the p–g–n heterostructure. d) Optical microscopy image of the device and the corresponding photocurrent mapping of the p–g–n device for V_{ds} = 0 V and V_g = 0 V. MoS_2, graphene, and WSe_2 are highlighted by yellow, light gray, and green dashed lines, respectively. The scale bar is 5 µm. Reproduced with permission.[123] Copyright 2016, American Chemical Society.

photodetectors with large responsivity and high sensitivity. In addition, the differences among atomically thin 2D materials in terms of their work functions, band gaps, and spin–orbit coupling strengths allow for the creation of various heterojunctions. By careful band alignment engineering and material selection, type II heterostructures and p–n junctions can be formed. This provides an ideal platform for the construction of self-powered photodetectors. Recently, Jiang et al. created a 2D GaTe–MoS_2 p–n heterojunction, in which MoS_2 is the n-type semiconducting material, with a hexagonal layered structure, and GaTe is the p-type semiconductor, with a less symmetric monoclinic structure (**Figure 6**a).[122] Although the heterojunction had an abrupt interface between the two completely dissimilar material systems, the resulting device exhibited excellent self-driven photoelectric characteristics. When the source–drain bias (V_{ds}) was set to 0 V, the source–drain current (I_{ds}) changed within <10 ms by repetitive switching on–off of the laser source, indicating the fast response and repeatability of the GaTe–MoS_2 heterostructure. As shown in Figure 6b, an on–off ratio of as high as 340 was achieved for this heterostructure, which is higher than those observed in individual GaTe (≈10) and individual MoS_2 (≈85). The authors attributed the excellent photodetection characteristics and self-driven photoswitching behavior to the type II band alignment and the existence of a built-in potential in the p–n heterojunction, which can efficiently separate the photogenerated electron–hole pairs. Upon illumination, the electrons and holes accumulated in MoS_2 and GaTe, respectively, leading to the formation of an open-circuit voltage. When the heterojunction operated under short-circuit conditions, the built-in potential drove the photogenerated electrons and holes, giving rise to self-driven photoswitching.

The design and construction of broadband photodetectors that can sense irradiation from the UV to infrared range is becoming a fast-growing field of interest in optoelectronic devices owing to its significant applications in image sensing, remote communication, and environmental monitoring. Recently, Miao et al. reported the successful application of a 2D heterojunction to achieve broadband photodetection in a self-powered mode. They sandwiched graphene (g) in an atomically thin p–n junction (WSe_2–MoS_2) to form a p–g–n heterojunction to realize broadband and high-sensitivity photovoltaic detectors (Figure 6c).[123] In this structure, graphene with a gapless band structure acted as an active material to absorb light over a large wavelength range. The built-in electric field at the interface of the p–n junction helps in separating the photogenerated electron–hole pairs and achieving broadband photodetection at zero bias voltage. In contrast to previously reported graphene-based photoconductive detectors, such a p–g–n heterojunction can largely depress the dark current, boost the specific detectivity and reduce the energy consumption. The heterojunction-based device exhibited a wide spectral photoresponse from 400 to 2000 nm at room temperature, with a specific detectivity of up to 10^{11} Jones in the near-infrared region. These results underscore the great potential of 2D vdW junctions for broadband detection applications in a self-powered mode. The authors also carried out a photocurrent mapping test by scanning a laser spot (830 nm with a power of ≈20.5 µW) over the device to gain insight into the photoresponse mechanism of the device. As seen from the photocurrent mapping at V_{ds} = 0 V and V_g = 0 V (Figure 6d), the overlapped field of MoS_2, graphene and WSe_2, not the electrode regions, showed the strongest photoresponse, suggesting that the photoresponse in this device originated from the well-designed atomically thin p–g–n junction, not from the metal contacts or other device regions.

In contrast to the p–n junction, there are different band alignments in the n–n homotype heterojunction such that

depletion and accumulation regions are created on opposite sides of the interface at thermal equilibrium, leading to majority carrier transport and enhancing the photoresponse speed of the device. In light of this, Jiang et al. reported the solution assembly of a 2D MoS_2 nanopetal/GaAs n–n homotype junction with graphene as the carrier collector.[119] The fabricated devices exhibited excellent photoresponse characteristics, including a high detectivity of up to 2.28×10^{11} Jones at zero bias and a very fast response speed (rise and decay times of 1.87 and 3.53 μs) with an extended photoresponse range (400–1300 nm). Additionally, the heterojunction could respond to fast pulse illuminations of up to 1 MHz, which is superior to the performances of current congeneric MoS_2-based photodetectors.

In this section, the advances in nanostructured p–n junctions with different configurations, such as core–shell, axial, crossed and branched structures, were summarized. In addition, the inorganic–organic p–n junction and 2D vdW heterostructures were adopted for applications as self-powered photodetectors.

4. Piezo-Phototronic Effect Enhanced Performances of Self-Powered Photodetectors

It is well known that wurtzite structured materials possess piezoelectric and semiconductor properties simultaneously. The typical wurtzite semiconductors include ZnO, CdSe, InN, and GaN. These materials show an anisotropic feature in the *c*-axis direction and perpendicular to the *c*-axis. Take ZnO as an example. The O^{2-} anions and Zn^{2+} cations are tetrahedrally coordinated, and their centers overlap with each other. When an external load is applied on an apex of a tetrahedron, the centers of the anions and cations are displaced relatively, resulting in a dipole moment. As a consequence, a piezoelectric field along the straining direction forms in the crystal owing to the accumulation of the dipole moments from all units. As long as pressure is applied, there is a piezopotential. The coupling of piezoelectric, semiconducting, and photoconductive properties opens up a new research field of piezo-phototronics, which was first proposed by Wang et al. in 2010.[124–127] The piezo-phototronic effect can utilize the piezopolarization charges to modulate/control carrier generation, separation, transport, and recombination by modifying the local electrical field distribution in the vicinity of the metal–semiconductor junction and homo-/heterojunction. This provides a promising strategy to enhance the performance of self-powered photodetectors.

4.1. Piezo-Phototronic Effect on the Schottky Junction

The built-in electric field created by the Schottky contact can separate the photogenerated electrons and holes, which gives rise to a photocurrent. According to the thermionic field emission theory, under irradiation of a certain power, the photocurrent is determined by the SBH, which can be tuned by the piezoelectric polarization.[128] One of the earliest related works was reported by Zhang et al. They transferred a single ZnO microwire onto a flexible polystyrene (PS) substrate, and one end of the microwire was contacted with an Au electrode to create a Schottky junction (**Figure 7**a).[129] Considering the intrinsic photoconductive and piezoelectric properties of ZnO, the effect of piezoelectric polarization on the photoresponse properties of the ZnO/Au Schottky junction was studied by applying different strains on the junction. It was found that both the sensitivity and photocurrent increased linearly with increasing tensile strain. When the device was loaded with a 0.580% tensile strain, five-fold enhancement of the sensitivity and 440% augmentation of the photocurrent were achieved (Figure 7b), whereas the response time, repeatability and stability of the sensor remained unchanged under strain. To explore the reason for the strain-enhanced performance of the device, the SBH was deduced at different tensile strains. It was

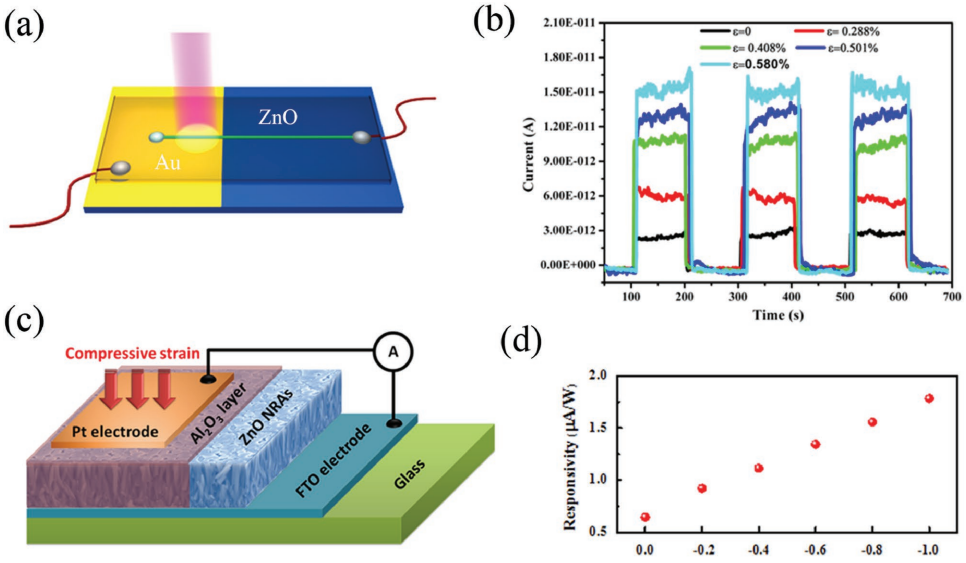

Figure 7. a) Schematic of the as-fabricated Au–ZnO Schottky junction. b) Time-dependent photoresponse as a function of strain. Reproduced with permission.[129] Copyright 2014, American Chemical Society. c) A schematic diagram of the Pt/Al_2O_3/ZnO nanorod array Schottky-junction-based photodetector. d) The photoresponsivity of the device under different compressive strains. Reproduced with permission.[130] Copyright 2014, Elsevier.

found that the SBH increased monotonically with increasing tensile strain, which is consistent with the variation trend of the photocurrent. The photoresponse enhancement under strain can also be explained from the viewpoint of the energy band diagram. Once external strain was applied on the ZnO wire, piezoelectric polarization charges were created because of the noncentral symmetric crystal structure of ZnO, which resulted in the redistribution of charges. Thus, the interface characteristics were modified by the remnant piezopotential. At the ZnO/Au interface, a negative piezopotential was formed, which drove the electron flow away from the interface, thus further depleting the interface and increasing the SBH. A wider and stronger built-in field is conducive to carrier separation and extraction, leading to an enhanced photoresponse. This study demonstrated that the piezo-phototronic effect can boost the performances of self-powered photodetectors based on Schottky junctions. Apart from single-nanowire-based Schottky junctions, piezo-phototronics can also be utilized to enhance the performance of nanowire-array-based junctions. A $Pt/Al_2O_3/ZnO$ nanorod array Schottky-junction-based self-powered photodetector was fabricated (Figure 7c).[130] The built-in electric field variation under the compressive strains induced by piezopolarization can effectively tune the SBH of the junction. As a result, the photoresponse performances of the device were greatly boosted via the SBH enhancement. Under a compressive strain of 1.0%, the photoresponsivity (Figure 7d) and specific detectivity of the device under zero bias voltage were enhanced by 2.77 and 2.78 times, respectively.

4.2. Piezo-Phototronic Effect on the p–n Junction

When the p–n junction is exposed to light irradiation, a large number of photoexcited electron–hole pairs are created. They will travel through the depletion region, driven by the built-in electric field, leading to a photocurrent. The piezo-phototronic effect can modulate the energy band profiles at the heterojunction interface and decrease/increase the barrier height, consequently tuning the photoresponse properties.

Recently, heterojunctions based on novel material combinations have been studied, such as ZnO/PEDOT:PSS, ZnO/spiro-MeOTAD, $Mg_xZn_{1-x}O$/Si p–n junctions, and ZnO/ZnS core/shell nanowires.[131–136] Zhang and co-workers fabricated a single ZnO nanowire and deposited p-type PEDOT:PSS on one end of the ZnO to form a p–n junction (**Figure 8**a).[131] Since the [0001] direction (+*c*-axis) points from ZnO to PEDOT, their interfaces formed a positive piezopotential when tensile strain was applied (Figure 8b). This lowered the conduction band level of ZnO and increased the barrier height, which led to the expansion of the depletion layer and the enhancement of the built-in field. Accordingly, the photoexcited electron–hole pairs were separated and transported more efficiently, leading to improved photocurrent and photosensitivity. Similar enhancement effects were also observed in ZnO/spiro-MeOTAD and CdS/P3HT junctions when external strain was applied.[18,132] Particularly for the latter one, the photocurrent under UV illumination of the junction was boosted to more than 330% when a 0.67% tensile strain was applied under the [001] direction point of the

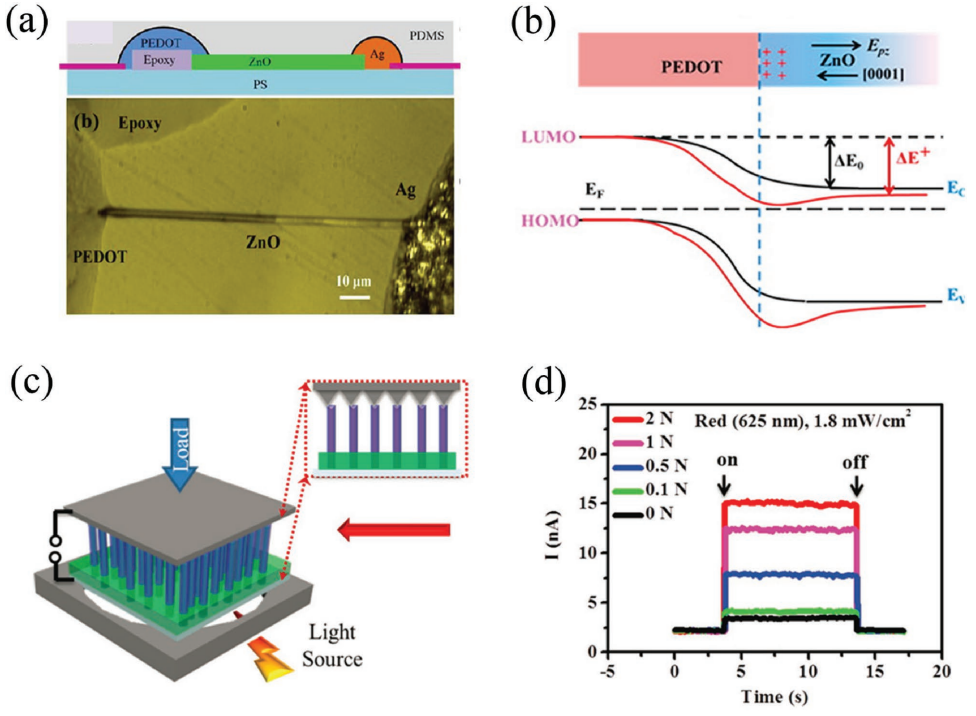

Figure 8. a) A schematic diagram of the PEDOT:PSS/ZnO heterojunction. b) Schematic energy band structures of the p–n junction in the presence and absence of strain. Reproduced with permission.[131] Copyright 2013, American Chemical Society. c) Schematic of a ZnO/ZnSe core/shell nanowire array photodetector. Inset is a schematic of Ag-coated flexible polyester with a zigzag structure on top of the nanowires as the top electrode. d) The photocurrent response of the device under different compressive loads without an external power source under a red excitation source. Reproduced with permission.[134] Copyright 2016, Wiley-VCH.

CdS microwire in contact with P3HT.[18] This enhancement can be ascribed to the increase of the built-in field at the interface of the p–n junction after the introduction of the piezo-phototronic effect, which is favorable for the separation of photogenerated electron–hole pairs in CdS and P3HT.

In the case of $Mg_xZn_{1-x}O$/Si, Mg was alloyed into a ZnO thin film to study how the alloying process and Mg content influence the piezoelectric coefficient and thus how the corresponding piezo-phototronic effect influences the performance improvement of photodetectors.[133] It was found that the increased Mg content enhanced the piezoelectric coefficient, thus increasing the piezopotential. As a result, more distinct performance enhancement was observed in the sample with higher Mg content. Another interesting work expands the application scope of the piezo-phototronic effect to a 3D core–shell nanowire array photodetector (Figure 8c).[134] A ZnO nanowire array was synthesized on ITO glass via a CVD method, followed by the deposition of a ZnSe shell through a pulsed-laser ablation process. Ag-coated polyester was deposited on the top of the core–shell array as the top electrode. It was found that with the increase of the compressive strain on the device, the photocurrent increased monotonously at no external bias (Figure 8d).

The recent progress in the piezo-phototronic effect enhanced performances of Schottky and p–n junction photodetectors is presented in this section. By introducing the piezopotential upon straining, the optoelectronic processes are modulated. The idea of using the piezo-phototronic effect to improve the photodetection performances has been demonstrated on devices ranging from a single nanowire device to a nanowire array photodetector. In addition, investigations have been carried out for diverse material systems and have greatly improved the understanding of piezo-phototronics. This promising technology provides a new platform for materials research and highly efficient optoelectronic device exploration.

5. Photoelectrochemical-Type Photodetectors

Emerging as a novel type of self-powered devices, PEC-type photodetectors have attracted wide attention. PEC-type photodetectors avoid the complicated lithography process and do not need external batteries as power sources, which makes them suitable for self-powered light detection.[59,60,137] Current research has been focused on the PEC-type UV photodetectors, and impressive results have been obtained. In this section, we will review the most important works on PEC-type self-powered photodetectors.

In 2011, Lee and co-workers first demonstrated a TiO_2/water solid-liquid heterojunction-based UV photodetector that consisted of two electrodes.[138] One was a 50 nm TiO_2 nanofilm coated on FTO glass. The other was 50 nm Pt deposited on an ITO substrate. They were assembled together using a sealant, and water was used as an electrolyte. Illuminated by 365 nm UV irradiation, the photocurrent of the device increased linearly with increasing light power intensity, indicating that the device was suitable for quantitative UV light detection. In addition, the device exhibited an excellent reproducible photoresponse to UV light while being blind to visible light, with a response time below 0.5 s and the highest responsivity of 69.2 mA W^{-1} at 350 nm. The superior capability for UV light detection of this device demonstrated the great potential of the PEC-type photodetector.

In 2012, a prototype of a PEC photodetector and the working mechanism were first formally proposed by Xie and co-workers (**Figure 9**a).[139] In this prototype, a nanocrystalline TiO_2 film coated on FTO glass as a photoanode was assembled with a Pt counter electrode into a sandwich cell, with I^-/I_3^- ionic liquid as the electrolyte. The working mechanism of the device is shown in Figure 9b. Upon UV light illumination, the TiO_2 nanofilm absorbs photons with energies above its bandgap, and electrons are excited from the valence band to the conduction band. Then, the photoexcited holes in the conduction band migrate to the semiconductor/electrolyte interface and oxidize the electrolyte (M) into an ionic species (M^+). The photoexcited electrons diffuse through the TiO_2 nanofilm and reach the surface of the FTO to become external circuit electrons (e), which flow to the counter electrode. Meanwhile, the formed M^+ ions diffuse through the electrolyte and arrive at the counter electrode. Then, the electrons at the counter electrode reduce the M^+ into M to complete the circuit.

Under 365 nm UV illumination (33 mW cm^{-2}), the short-circuit current reached 550 μA cm^{-2}, which corresponds to a photoresponsivity of 16.7 mA W^{-1}. In a broad UV light intensity region (25 μW cm^{-2} to 33 mW cm^{-2}), the current increased linearly with the increase of the light power intensity. A reproducible photoresponse under repeating cycles of UV light with on–off ratios of up to 269.8 was achieved for this device at zero bias voltage. The rise time and decay time were measured to be ≈0.08 and 0.03 s, respectively (Figure 9c). The as-fabricated device exhibited an obvious UV response, with the highest response at ≈330 nm (Figure 9d). These results suggest that the PEC-type photodetector can achieve light detection without an external power source. This successfully opens up new platforms for self-powered photodetectors. Since then, many scientists have devoted themselves to fabricating various PEC-type photodetectors.

The studies on improving the performances of PEC-type photodetectors have focused on developing highly efficient photoanodes. Similar to dye-sensitized solar cells, there are several approaches for improving the performances of photoanodes: strengthening the light harvesting ability, depressing the recombination rate or improving the charge separation, and speeding up the charge transport. In light of this, various nanostructures have been developed and utilized as photoanodes.

The hierarchical branched nanostructure is one promising structure that provides strong light absorption for the photodetectors. Chen et al. fabricated branched TiO_2 arrays on a FTO substrate via a simple process and applied them as photoanodes to assemble a PEC photodetector (**Figure 10**a).[140] It has been reported that the branched nanoarrays generally have a larger specific surface area and exhibit higher light absorption and better charge transport characteristics than nanoparticle films. In contrast to bare TiO_2 nanorod-array-based photodetectors, TiO_2 branched nanoarrays with a reaction time of 18 h exhibited drastically improved photodetection performance as photoanodes (Figure 10b). Under 365 nm UV light irradiation, the device exhibited a high photocurrent density of 373 μA cm^{-2}, corresponding to a photoresponsivity of 186.5 mA W^{-1}, which

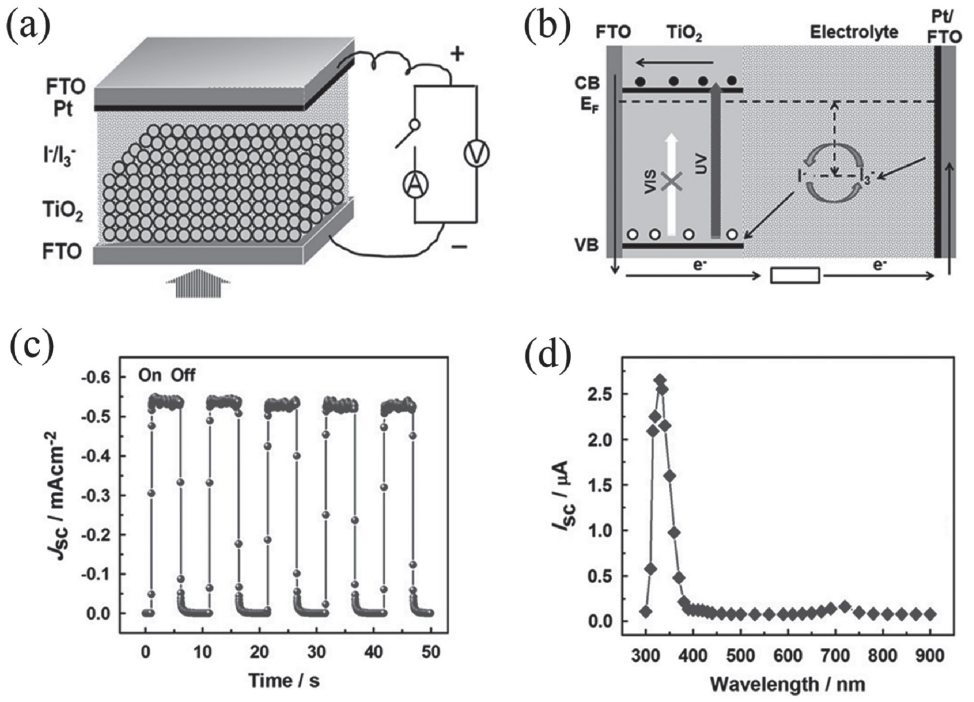

Figure 9. a) Schematic of the PEC-type self-powered UV photodetector. b) The working mechanism of the device. c) Time responses of the short-circuit current upon 365 nm UV light illumination measured for light-on and light-off states. d) The spectral responses of the device. Reproduced with permission.[139] Copyright 2012, Elsevier.

was much higher than that of the abovementioned nanocrystalline TiO_2 films. Moreover, a fast photoresponse speed (rise time of 0.15 s and decay time of 0.05 s) was achieved for this device. The superior performances of this branched arrays can be attributed to three reasons: the branches filled the spaces between the nanorods, which enhanced the light harvesting ability; the 1D single-crystalline TiO_2 nanorod enabled the fast transport of photogenerated electrons from TiO_2 branches to the collecting FTO substrates; and the increased surface area of TiO_2 nanobranched arrays resulted in enlarged TiO_2/electrolyte contact areas. Another interesting work concerns the TiO_2/SnO_2 branched nanostructure consisting of TiO_2 branches and SnO_2 nanofiber networks (Figure 10c).[141] It serves as an ideal configuration for a PEC-type self-driven UV photosensor. The nanostructures not only provide a direct pathway for electron transport but also offer a low charge recombination rate. Under UV light illumination, the self-driven UV sensor exhibited a high responsivity of 0.6 A W^{-1}, a large on/off ratio of 4550 and rise and decay times of 0.03 and 0.01 s, which were superior to those of TiO_2- and SnO_2-based devices (Figure 10d).

Interfacial charge recombination causes the loss of photogenerated electrons, which is a big problem in PEC-type photodetectors, as it strongly restricts the photodetection performance.[142] Recently, core–shell semiconductor nanostructures with type II band alignments have been developed and fabricated as photoanodes because they facilitate rapid carrier separation. In such structures, the conduction band energy of the shell material should be more negative than that of the core material. As a result, the semiconductor/electrolyte interface will form an energy barrier, which is beneficial for the separation of photogenerated carriers, accordingly depressing interfacial charge recombination. In light of this, various core–shell structures, such as ZnO–TiO_2, ZnO–NiO, and ZnO–ZnS, have been fabricated as photoanodes to construct high-performance PEC self-powered photodetectors.[143–145]

Xie and co-workers reported a photoanode built from ZnO/TiO_2 core–shell nanostrawberries in 2013.[143] Upon 365 nm UV irradiation, the core–shell-structure-based device gave rise to a high short-circuit current of 357 μA cm^{-2} with a photoresponsivity of 17.85 mA W^{-1}, representing 52.5% enhancement compared to that for pristine ZnO. The photosensitivity of the ZnO–TiO_2 core–shell structure was ≈37900, which was 3.24 times higher than that of pristine ZnO. The rise and decay times were calculated to be 0.022 and 0.009 s for this device, respectively. A linear increase of the photocurrent with increasing UV light intensity (from 0.002 to 40 mW cm^{-2}) was observed. In addition to TiO_2, other materials, including ZnS and NiO, have been utilized to improve the efficiencies of ZnO-based photoanodes. NiO, as a p-type semiconductor, can be integrated with ZnO to form a p–n junction and create a built-in electric field at their interface. NiO/ZnO core–shell nanorod arrays were successfully constructed by Dai and co-workers, and they found that the photosensitivity of the device was as high as 167, which represents a 49-fold enhancement compared with the bare ZnO nanorods.[144] Furthermore, both the rise and decay times of this core–shell device were greatly reduced. As a wide-bandgap semiconductor with relatively higher conduction band position, ZnS is also suitable for integration with ZnO to form a type II alignment. Guo et al. fabricated ZnO/ZnS nanorod arrays and studied their photodetection performance.[145] It was

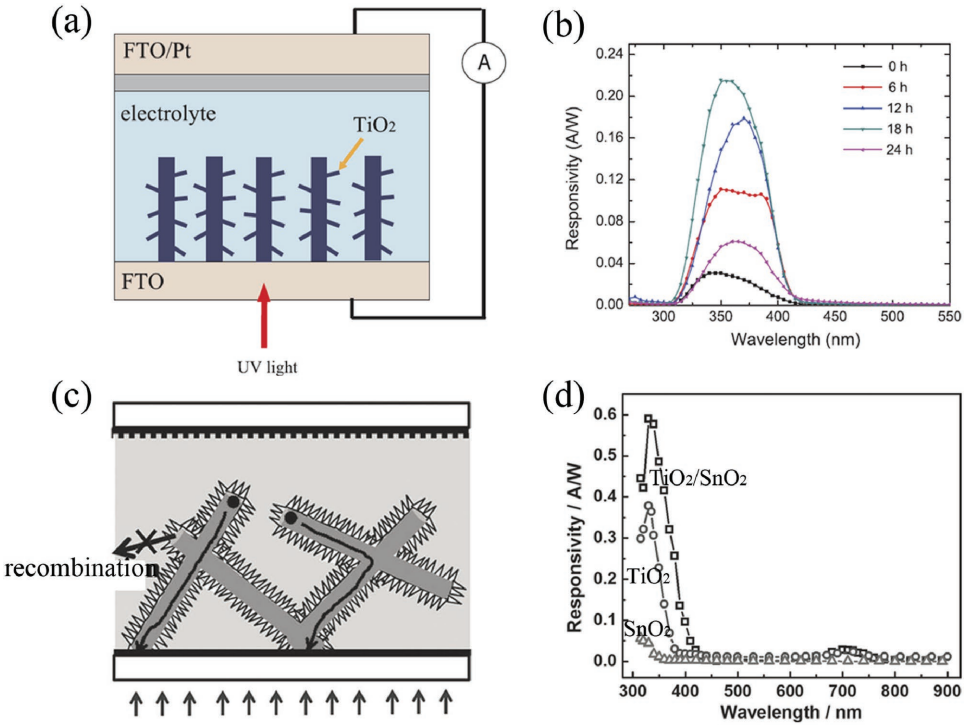

Figure 10. a) Schematic diagram of PEC-type photosensors built from TiO_2 branched nanoarrays. b) Spectral responsivities of devices based on the as-fabricated TiO_2 branched arrays with various reaction times (0, 6, 12, 18, 24 h) under zero bias voltage. Reproduced with permission.[140] Copyright 2014, IOP Publishing Ltd. c) Diagram for the PEC-type photodetector based on TiO_2–SnO_2 branched nanostructures. d) The comparative spectral responsivities of TiO_2–SnO_2-, TiO_2-, and SnO_2-based devices. Reproduced with permission.[141] Copyright 2013, Wiley-VCH.

found that under UV illumination at zero bias, the photocurrent of the ZnO/ZnS nanorod arrays doubled compared to that of ZnO, which was attributed to the efficient charge separation due to the type II alignment.

In this section, the recent advances in PEC-type self-powered photodetectors have been briefly summarized. Various nanostructures, including nanocrystalline films, nanowire arrays, and branched and core–shell nanostructures, have been designed and fabricated for photoanodes of PEC-type detectors, benefiting from their high light absorption and fast carrier separation/transport efficiencies. As a consequence, PEC-type photodetectors with high spectral responsivity, large photosensitivity, and fast photoresponse have been developed.

6. Integrated Self-Powered Nanosystems

Harvesting different forms of energies from nature to build self-powered nanosystems is emerging as a research hotspot.[146–148] Many kinds of energy, such as chemical energy, thermal energy, mechanical energy, and solar energy, can be scavenged from the environment by energy harvesters.[149–152] The output power ranges from microwatt to milliwatt, which can effectively power a micro/nanodevice. Generally, a self-powered nanosystem for light detection is composed of three components: a light sensor, a power unit and an electrical measurement system. A photodetector could either be assembled with an energy harvester unit (a nanogenerator or solar cell) or be combined with an energy storage unit (a lithium ion battery or supercapacitor) to drive these components.

Nanogenerators, invented by Wang et al., rely on the piezoelectric potential formed in the nanowire via an applied load: owing to the driving force of the piezopotential, a dynamic straining of the nanowire leads to a transient electron flow under external pressure. Various types of mechanical energy sources have been scavenged by nanogenerators, including air flow, liquid flow, and mechanical vibrations.[153,154] In the past decade, Wang and co-workers have focused on developing a nanogenerator technology for constructing a self-driven nanosystem. Self-powered nanosystems have been realized in pH sensors, laser diodes, pressure sensors, temperature sensors, etc.[65,147,148,155–157] The great advances in nanogenerator technologies provide great opportunities and push forward the study of self-driven nanosystems, particularly for light detection systems.

Wang and co-workers reported the first demonstration of a self-driven nanosystem, in which a UV photosensor was powered by a nanogenerator.[65] They fabricated a vertically or laterally aligned ZnO-nanowire-array-based high-power-output nanogenerator. When a uniaxial strain was periodically applied to the ZnO nanowire array, a piezoelectric potential along the nanowires was created, resulting in an alternating electrical output. An enhanced output voltage of 0.243 V was achieved for an integrated nanogenerator by using a three-layer integration of the vertical nanowire array. This nanogenerator was coupled with an individual ZnO-nanowire-based UV photodetector

to form a self-driven nanosystem, in which the two components were connected in series to create a loop. A voltmeter was used to monitor the voltage across the photodetector. The working mechanism of this nanosystem is as follows: In the dark, the resistance of the UV detector is large because of the inner resistance of the nanogenerator, which gives rise to a large voltage drop on the detector. Upon UV light illumination, its resistance remarkably reduces, which results from the increasing carrier concentrations; thus, the voltage drop on the detector also decreases in magnitude. The above result indicates that the nanogenerator can power a nanodetector to detect UV light. With the development of nanogenerator technology, a larger output power, with 6 V voltage and 45 nA current, has been achieved for a nanogenerator based on lead zirconate titanate nanowires.[66] By integrating this nanogenerator with a ZnO UV detector, quantitative UV light detection over a wide range can be achieved for this flexible self-powered nanosystem (**Figure 11**a,b).

As shown in the above studies, a nanogenerator can be used as a power source to drive a photodetector. Alternatively, the nanogenerator can be directly used as a sensor to detect light illumination. Recently, a fully integrated UV light sensor was built from a triboelectric nanogenerator (Figure 11c), in which 3D dendritic TiO_2 nanostructures were employed not only as the contact material of the nanogenerator but also as the built-in photodetectors.[158] By using poly(methylmethacrylate) and a spring to integrate the triboelectric nanogenerator-based photosensor, a self-driven nanodevice was realized. Via a periodic impact on the device due to finger tapping, a fast response speed (rise and decay times of 18 and 31 ms), a high photoresponsivity approaching 280 A W^{-1}, and a broad linear detection range (20 μW cm^{-2} to 7 mW cm^{-2}) were obtained (Figure 11d).

Microbial fuel cell (MFCs), which convert chemical energy into electricity, have several advantages over conventional batteries, including a higher energy storage density and more rapid recharging.[159] Thus, it is possible to integrate MFCs with a photodetector to build a high-performance self-powered system. **Figure 12**a shows an integrated system, in which a self-driven sensitive nanowire-based multicolor photosensor was driven by an MFC that was built from a carbon fiber-ZnO nanowire hybridized structure.[63] Interestingly, one microscale MFC is able to drive a CdS nanowire sensor to detect light, with a high photoresponsivity and an ultralow detection limit. When UV light (1.6×10^{-4} W cm^{-2}) was illuminated on the CdS nanowire, the nanosystem current quickly increased to 1.4 nA. The nanosystem can also detect multicolored light ranging from UV light to red light with a detection limit as low as several nW cm^{-2}.

A solar cell is an electrical device that transforms solar energy directly into electricity, which provides renewable and clean energy. It can also act as an integrated power source for self-driven nanosystems. Recently, organic-inorganic hybrid perovskites have been widely used in solar cells and photodetectors due to their fascinating optical and electrical properties.[160,161] Our group first assembled an all-perovskite self-powered nanosystem by coupling a perovskite solar cell with a perovskite photodetector (Figure 12b).[64] The solar cell in the nanosystem, as an energy conversion unit, can provide a voltage of 0.93 V for the photodetector under AM1.5 irradiation (100 mW cm^{-2}). The typical photoresponse of the photodetector under periodic on–off light irradiation revealed that the nanosystem exhibited a stable and fast response to light irradiation. This integrated system exhibited light detection ability similar to that of a normal photosensor powered by an external power source.

Some energy sources, such as solar and wind energies, are intermittent. As a result, variances in time and space interrupt the harvesting of these energies, leading to unstable output power in solar cells and nanogenerators. Alternatively, lithium ion batteries and supercapacitors, as energy-storage devices, can provide a stable and durable output.[162,163] For this reason, they have been integrated with light sensors to form a self-powered nanosystem. Shen and co-workers have reported a series

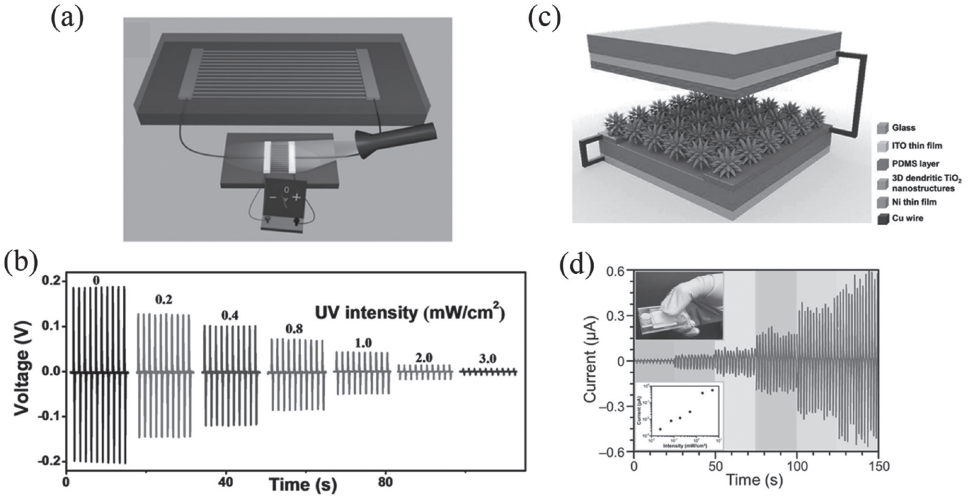

Figure 11. a) Schematic of a self-driven system composed of a UV sensor and a nanogenerator. b) Photoresponses of the nanosystem under UV light with different power intensities. Reproduced with permission.[65] Copyright 2012, American Chemical Society. c) A schematic diagram of a nanogenerator based on dendritic TiO_2 nanostructures. d) Output current of the device triggered by biomechanical movements under UV light illumination with different power intensities. Insets are a photograph of the device and the dependence curve of the output current on the incident light intensity. Reproduced with permission.[158] Copyright 2014, Wiley-VCH.

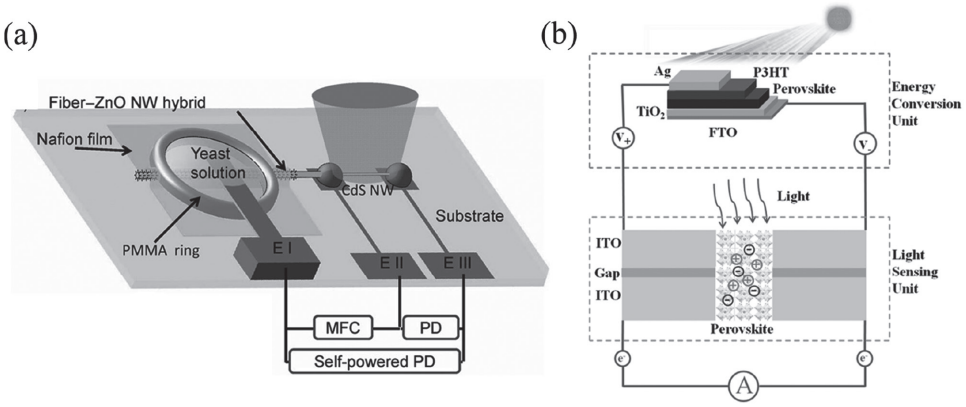

Figure 12. a) Schematic illustration of a self-driven system composed of an MFC and a nanowire photodetector. Reproduced with permission.[63] Copyright 2012, Wiley-VCH. b) Schematic illustration of a self-powered all-perovskite photodetector-solar cell nanosystem. Reproduced with permission.[64] Copyright 2016, Wiley-VCH.

of works in this field.[67,164,165] They began with the assembly of a self-powered photodetector nanosystem by integrating a UV photodetector with a lithium-ion battery based on SnO_2 cloth.[164] Then, they fabricated an asymmetric all-solid-state supercapacitor that can accomplish light detection and energy storage simultaneously, in which graphene was used as both the light-active material and negative electrodes and Co_3O_4 nanowires as the positive electrodes.[165] One recent report described an on-chip integrated photosensing nanosystem, which consisted of a reduced graphene oxide-based in-plane micro supercapacitor and a CdS nanowire photosensor.[67] In this structure, the electrodes in the micro supercapacitor were employed as the drain and source electrodes of the CdS photosensor.

With the rapid development of portable devices and electronic products, multifunctional integrated nanodevices, which couple various functions into one device and miniaturize the volume, have been rapidly developed in recent years. In particular, artificial electronic skins (e-skins), which can mimic human skin to sense various physical stimuli, including light, temperature, strain, humidity, and environmental gases, are attracting much attention and emerging as a research hotspot.[166,167] Significantly, the power units also need to be integrated into the multifunctional e-skins to form self-powered nanosystems, which are especially favorable for next-generation multifunctional e-skins. Recently, a novel self-powered e-skin for image recognition was realized from a pixel-addressable matrix of piezo-phototronic ZnO nanowire arrays.[168] The skin can actively output piezoelectric voltage under an applied deformation. In addition, the UV illumination intensity greatly affects the output piezoelectric voltage, indicating that the e-skin can be applied as an active photodetector to sense UV light. More importantly, no external power source is required for the e-skin. In addition, image recognition is realized by using an e-skin with a 6×6 pixel-addressable matrix, which is able to map multipoint UV stimuli. Recently, a multifunction self-powered e-skin system was successfully fabricated, which consisted of four devices: micro-supercapacitors, a pressure sensor, a photodetector, and a gas sensor.[169] Driven by the micro-supercapacitors, the e-skin can detect pressure, light and gas simultaneously, similar to the functions of human skins and sensory organs. This work demonstrated the great potential of rationally designed integrated self-powered nanosystems for application to next-generation wearable electronics and artificial intelligence fields.

In this section, the energy-harvesting techniques and their prospects for application in self-powered photodetectors are discussed. The successful development of energy-harvesting nanodevices that can sustainably and stably operate over a broad range of conditions enables their integration with photodetectors to form self-powered nanosystems. Moreover, multifunctional integrated nanodevices that can perform in a self-powered mode, which have great potential in next-generation electronic devices, have attracted wide research interest.

7. Advantages and Disadvantages of Different Types of Photodetectors

Each type of self-powered photodetector has its own advantages and disadvantages. We try to summarize the characteristics of each kind of self-powered photodetector. A systematic comparison among them is provided in terms of fabrication process, performance parameters, long-term stability, and flexibility.

As for the fabrication processes, the Schottky junction avoids a complex process due to its simple device structure. One can deposit a metal electrode on one end of the nanowire or nanoarray to form a Schottky junction, while for a p–n junction, a doping process is required to obtain a p-type semiconductor. Particularly for the fabrication of core–shell and branched p–n junctions, a combination process with at least two steps is usually used. For the PEC-type photodetector, photoanodes are first fabricated via a physicochemical route. Then, they are assembled with a counter electrode into a sandwich cell. The integrated nanosystem requires a complex fabrication process: first, the energy harvesting unit and light sensing unit are fabricated; then, they are connected into a loop.

Most of the reported Schottky and p–n junctions are built from a single nanowire or a single-layer nanosheet, resulting in output current signals on the order of nA or μA; thus, high-precision galvanometers are needed to detect the current. In contrast, a PEC-type photodetector can generate a large current, up to mA, due to the large active area of the photoanodes. It is well known

that the photoresponsivity and photosensitivity are affected not only by the device structure but also by the morphologies and compositions of the materials. However, according to the results of previous works, the p–n junction and Schottky junction generally exhibit higher performances in terms of photosensitivity and photoresponsivity compared with the PEC detector and integrated system. Additionally, their performances can be further enhanced by exploiting the piezo-phototronic effect. As for the response speed, the Schottky junction and p–n junction outperform the PEC cell and integrated nanosystem. Due to the short travel length and fast charge transport in the Schottky and p–n junctions, fast response speeds can be achieved, while for the PEC photodetector, the response time mainly includes two parts: the time taken by the electrons at the solid/electrolyte interface to diffuse to the FTO substrate through the semiconductor film and the time taken by the oxidized redox species to drift to the counter electrode through the electrolyte. This results in a lower response speed compared with the Schottky junction and p–n junction. For the integrated nanosystem, the light sensor unit is usually based on the photoconductivity effect of the nanostructure, which gives rise to medium response speed.

Stability is one of the most important issues for a photodetector, which determines the lifespan of the device and is important for practical applications. For PEC photodetectors, the I^-/I_3^- redox couple is normally used as the electrolyte. However, the I^-/I_3^- redox couple is highly volatile, corrosive and photoreactive. It can interact with metallic components and sealing materials, strongly limiting the long-term operation of PEC photodetectors. In contrast, after exposure to atmospheric conditions over a long time, the Schottky junction and p–n junction still maintain their initial performances, as was demonstrated in the work on ZnO/CuSCN.[101]

Compared with rigid devices based on a silicon substrate, the flexible photodetectors have a wider application scope in the field of wearable and portable devices owing to their reduced weights and better mechanical flexibility.[166] It has been demonstrated that the Schottky junction and p–n junction are compatible with flexible substrates, while for the PEC cell, it is difficult to achieve flexibility because of the device configuration. For the integrated nanosystem, wearable and flexible devices have been demonstrated.[170]

8. Conclusion

In summary, the most important advances in self-powered photodetectors were overviewed. Different types of self-powered photodetectors, including those based on the Schottky junction, p–n junction and PEC cell, were fabricated by exploiting the photovoltaic effect. In addition, by introducing the piezo-phototronic effect into the Schottky junction and p–n junction, enhanced performances were realized. As an alternative approach to achieving light detection, an integrated nanosystem was developed, which can work in a self-powered mode. To present a clear comparison, the key parameters for various self-powered photodetectors and integrated nanosystems in previous reports are summarized in **Table 1**.

Despite the great progress that has been made for the photodetectors based on Schottky and p–n junctions, the performance parameters of self-powered photodetectors should be further enhanced to realize practical applications. First, to the best of our knowledge, currently, the fastest response speed of a p–n junction is 4 ns, which was reported by Dunn et al.[101] However, for some unique applications, such as in the aeronautical and space fields, faster response speeds, down to ps, are desired. Thus, more work needs to be done to further enhance the response speed by adjusting the material morphologies and compositions in the junctions. Second, the weak light detection ability of the photodetectors needs to be further enhanced. The current experimental results on most photodetectors reveal that the light-intensity detection limits are still very high. However, for optical communications and environmental monitoring, excellent detection ability for weak light is highly needed. Third, novel strategies should be developed to remarkably reduce the size and weight of self-powered photodetectors. Mechanical flexibility is also desired for some particular applications. Once these issues have been properly addressed, sustainable self-powered photodetectors will play a significant role in the advancement of many fields, such as imaging techniques, light-wave communications, medical science, and defense technology. Last but not least, piezo-phototronics provides a great opportunity to improve the photodetection performance of the Schottky and p–n junction photodetectors. The three-way coupling and the controllable tuning characteristics make piezo-phototronics very powerful for introducing new vitality into traditional optoelectronic devices and exploring devices with novel working principles. The last few years have witnessed the rapid progress of piezo-phototronics. The extended material systems and deeper understanding of piezo-phototronics will contribute to the performance enhancement of self-powered photodetectors. Additional research efforts are needed to further realize the huge potential of piezo-phototronics.

Regarding the PEC-type photodetector, stability is an essential issue that needs additional research efforts. Currently, few works are focused on the systematic investigation of the stability of PEC photodetectors. As stated above, compared to the Schottky or p–n junctions, PEC-type photodetectors generally exhibit inferior stability, which is mainly due to the utilization of a volatile electrolyte, the photocorrosion of the semiconductor, etc. Accordingly, a series of systematic works should be carried out to enhance the long-term stability of PEC-cell-based photodetectors in the future. As an alternative to the I^-/I_3^- redox couple, water is an ideal candidate for the electrolyte in PEC photodetectors because water is a safe, stable, and environmentally friendly electrolyte. Recently, a TiO_2/water solid–liquid heterojunction-based photodetector was developed.[137] Interestingly, this device exhibited decent photosensitivity, a fast response and high spectral selectivity. Apart from liquid electrolytes, a quasi-solid-state electrolyte is suitable for the PEC device because of the greatly improved stability and sealing ability, which is beneficial for practical applications. However, the efficiencies of the photodetectors with aqueous electrolytes or quasi-solid-state electrolytes are usually inferior compared to the devices with I^-/I_3^- electrolytes. Thus, further research into the development of PEC-type photodetectors with aqueous and quasi-solid-state electrolytes is required to achieve enhanced performances and long-term stability.

Table 1. Comparison of the key parameters for self-powered nanoscale photodetectors in previous report.

Materials	Device type	On–off ratio	Responsivity [mA W^{-1}]	Detectivity [Jones]	Response time	Reference
Sb-doped ZnO/Au	Schottky	22	–	–	100 ms	[43]
Ga-doped CdS/Au	Schottky	10^3	8×10^3	–	95/290 µs	[47]
ZnO nanowire array/Pt	Schottky	1.7×10^4	1.82	–	81/95 ms	[45]
PbS quantum dots/In	Schottky	10^3	2×10^2	–	0.8/3.2 µs	[41]
Ga_2O_3 nanowire array/Au	Schottky	–	1×10^{-2}	–	1/64 µs	[42]
TiO_2/Au/TiO_2	Schottky	–	10^3	–	0.37/6.6 s	[78]
CdSe nanobelt/graphene	Schottky	3.5×10^5	1.62×10^4	–	82/179 ms	[53]
Ge/graphene	Schottky	1×10^4	51.8	1.38×10^{10}	23/108 µs	[48]
Si/graphene	Schottky	–	4×10^2	5.4×10^{12}	–	[50]
Si/graphene	Schottky	3.5×10^7	7.3×10^2	5.77×10^{13}	–	[51]
ZnO nanowire homojunction	p–n	10^6	–	–	30/50 ms	[98]
Black phosphorus	p–n	–	6.2	–	3/12 ms	[16]
ZnO/GaN	p–n	2×10^6	–	–	20/219 µs	[100]
ZnO/CuSCN	p–n	–	7.5	–	4 ns/6.7 µs (0.1 mV)	[101]
ZnO/NiO	p–n	–	4.2×10^{-2}	1.1×10^9	1.2/7.1 s	[17]
In_2Se_3/Si	p–n	–	5.67×10^3	5.66×10^{13}	175/226 µs	[58]
CdS/Si	p–n	21.1	1.1×10^2	–	–	[106]
N:ZnO-SpiroMeOTAD	p–n	1.6×10^4	6.5	–	200/950 µs	[116]
ZnO/PVK	p–n	2	9.96	–	1.5/6 s	[118]
MoS_2/GaAs	n–n	–	–	2.28×10^{11}	1.87/3.53 µs	[119]
ZnO/Ga_2O_3	n–n	–	9.7	2.58×10^{12} (–0.1 V)	100/900 µs	[171]
TiO_2 nanocrystalline film	PEC type	–	16.7	–	80/30 ms	[139]
TiO_2 branched nanoarray	PEC type	–	1.87×10^2	–	150/50 ms	[140]
TiO_2/SnO_2 branched nanostructure	PEC type	4.55×10^3	6×10^2	–	30/10 ms	[141]
ZnO/TiO_2 core–shell nanostrawberries	PEC type	3.79×10^4	17.85	–	22/9 ms	[143]
TiO_2 based triboelectric nanogenerator	Nanosystem	–	2.8×10^5	–	18/31 ms	[158]
MFC/nanosensor	Nanosystem	–	1.18×10^6	–	–	[159]
Perovskite solar cell-photodetector	Nanosystem	1.73×10^2	–	–	2.2/0.3 s	[64]
micro supercapacitor/CdS nanowire photosensor	Nanosystem	79.81	–	–	0.83/2.9 s	[67]

As for integrated nanosystems, to meet the demands of practical applications, an energy harvesting unit with sufficiently high and more stable outputs should be developed. In addition, future endeavors are needed to achieve flexible visual and multifunctional nanosystems, especially e-skins, which will significantly broaden the application scope. The self-powered technique is a new paradigm in nanotechnology for truly achieving sustainable self-sufficient micro/nanosystems, which are of great importance for sensing, medical science, infrastructure/environmental monitoring, defense technology, and wearable electronics. It is anticipated that self-powered nanosystems will play a key role in our daily lives in the near future.

Acknowledgements

The authors acknowledge the support from the National Natural Science Foundation of China (51772197, 51422206, 51372159, 51502184), Key University Science Research Project of Jiangsu Province, 1000 Youth Talents Plan, 333 High-level Talents Cultivation Project of Jiangsu Province, Six Talents Peak Project of Jiangsu Province, Distinguished Young Scholars Foundation by Jiangsu Science and Technology Committee (BK20140009), Natural Science Foundation of Jiangsu Province (BK20150331), and Funded by the Priority Academic Program Development of Jiangsu Higher Education Institutions (PAPD).

Conflict of Interest

The authors declare no conflict of interest.

Keywords

junctions, optical sensors, photodetectors, photoresponse, self-powered

Received: June 1, 2017
Revised: August 2, 2017
Published online:

[1] J. Zhu, M. C. Hersam, *Adv. Mater.* **2017**, *29*, 1603895.
[2] F. L. Yuan, Z. B. Wang, X. H. Li, Y. C. Li, Z. A. Tan, L. Z. Fan, S. H. Yang, *Adv. Mater.* **2017**, *29*, 1604436.
[3] Z. Y. Yang, O. Voznyy, M. X. Liu, M. J. Yuan, A. H. Ip, O. S. Ahmed, L. Levina, S. Kinge, S. Hoogland, E. H. Sargent, *ACS Nano* **2015**, *9*, 12327.
[4] S. R. Zhao, H. P. T. Nguyen, M. G. Kibria, Z. T. Mi, *Prog. Quantum Electron.* **2015**, *44*, 14.
[5] C. Couteau, A. Larrue, C. Wilhelm, C. Soci, *Nanophotonics* **2015**, *4*, 90.
[6] Y. Y. Zhang, J. Wu, M. Aagesen, H. Y. Liu, *J. Phys. D: Appl. Phys.* **2015**, *48*, 463001.
[7] Z. H. Wang, B. Nabet, *Nanophotonics* **2015**, *4*, 491.
[8] Y. Zhao, Q. Han, Z. H. Cheng, L. Jiang, L. T. Qu, *Nano Today* **2017**, *12*, 14.
[9] J. Shim, H. Y. Park, D. H. Kang, J. O. Kim, S. H. Jo, Y. Park, J. H. Par, *Adv. Electron. Mater.* **2017**, *3*, 1600364.
[10] S. L. Yu, X. Q. Wu, Y. P. Wang, X. Guo, L. M. Tong, *Adv. Mater.* **2017**, *29*, 1606128.
[11] N. P. Dasgupta, J. W. Sun, C. Liu, S. Brittman, S. C. Andrews, J. Lim, H. W. Gao, R. X. Yan, P. D. Yang, *Adv. Mater.* **2014**, *26*, 2137.
[12] S. Barth, F. Hernandez-Ramirez, J. D. Holmes, A. Romano-Rodriguez, *Prog. Mater. Sci.* **2010**, *55*, 563.
[13] X. J. Feng, K. Shankar, O. K. Varghese, M. Paulose, T. J. Latempa, C. A. Grimes, *Nano. Lett.* **2008**, *8*, 3781.
[14] A. K. Geim, K. S. Novoselov, *Nat. Mater.* **2007**, *6*, 183.
[15] A. Pospischil, M. M. Furchi, T. Mueller, *Nat. Nanotechnol.* **2014**, *9*, 257.
[16] Y. Liu, Y. Cai, G. Zhang, Y. W. Zhang, K. W. Ang, *Adv. Funct. Mater.* **2017**, *27*, 1604638.
[17] L. Zheng, F. Teng, Z. Zhang, B. Zhao, X. Fang, *J. Mater. Chem. C* **2016**, *4*, 10032.
[18] X. X. Yu, H. Yin, H. X. Li, W. Zhang, H. Zhao, C. Li, M. Q. Zhu, *Nano Energy* **2017**, *34*, 155.
[19] X. S. Fang, T. Y. Zhai, U. K. Gautam, L. Li, L. M. Wu, Y. Bando, D. Golberg, *Prog. Mater. Sci.* **2011**, *56*, 175.
[20] H. Kind, H. Q. Yan, B. Messer, M. Law, P. D. Yang, *Adv. Mater.* **2002**, *14*, 158.
[21] F. N. Xia, T. Mueller, Y. M. Lin, A. Valdes-Garcia, P. Avouris, *Nat. Nanotechnol.* **2009**, *4*, 839.
[22] G. Konstantatos, E. H. Sargent, *Nat. Nanotechnol.* **2010**, *5*, 391.
[23] C. Soci, A. Zhang, B. Xiang, S. A. Dayeh, D. P. R. Aplin, J. Park, X. Y. Bao, Y. H. Lo, D. Wang, *Nano Lett.* **2007**, *7*, 1003.
[24] F. H. L. Koppens, T. Mueller, P. Avouris, A. C. Ferrari, M. S. Vitiello, M. Polini, *Nat. Nanotechnol.* **2014**, *9*, 780.
[25] T. Y. Zhai, X. S. Fang, M. Y. Liao, X. J. Xu, H. B. Zeng, Y. Bando, D. Golberg, *Sensors* **2009**, *9*, 6504.
[26] T. Y. Zhai, L. Li, Y. Ma, M. Y. Liao, X. Wang, X. S. Fang, J. N. Yao, Y. Bando, D. Golberg, *Chem. Soc. Rev.* **2011**, *40*, 2986.
[27] W. Tian, H. Lu, L. Li, *Nano Res.* **2015**, *8*, 382.
[28] K. M. Deng, L. Li, *Adv. Mater.* **2014**, *26*, 2619.
[29] U. Otuonye, H. W. Kim, W. D. Lu, *Appl. Phys. Lett.* **2017**, *110*, 173104.
[30] L. D. Li, L. L. Gu, Z. Lou, Z. Y. Fan, G. Z. Shen, *ACS Nano* **2017**, *11*, 4067.
[31] Q. F. Liu, M. Gong, B. Cook, D. Ewing, M. Casper, A. Stramel, J. Wu, *Adv. Mater. Interfaces* **2017**, *4*, 1601064.
[32] J. Yu, N. Tian, *Phys. Chem. Chem. Phys.* **2016**, *18*, 24129.
[33] K. M. Azizur-Rahman, R. R. LaPierre, *Nanotechnology* **2016**, *27*, 315202.
[34] X. Yan, B. Li, Y. Wu, X. Zhang, X. M. Ren, *Appl. Phys. Lett.* **2016**, *109*, 053109.
[35] Q. S. Wang, J. Li, Y. Lei, Y. Wen, Z. X. Wang, X. Y. Zhan, F. Wang, F. M. Wang, Y. Huang, K. Xu, J. He, *Adv. Mater.* **2016**, *28*, 3596.
[36] Z. L. Wang, *Adv. Funct. Mater.* **2008**, *18*, 3553.
[37] Z. L. Wang, W. Z. Wu, *Angew. Chem., Int. Ed.* **2012**, *51*, 11700.
[38] Z. L. Wang, *ACS Nano* **2013**, *7*, 9533.
[39] L. Peng, L. F. Hu, X. S. Fang, *Adv. Funct. Mater.* **2014**, *24*, 2591.
[40] Z. Bai, X. Yan, X. Chen, H. Liu, Y. Shen, Y. Zhang, *Curr. Appl. Phys.* **2013**, *13*, 165.
[41] L. Mi, H. Wang, Y. Zhang, X. Yao, Y. Chang, *Nanotechnology* **2017**, *28*, 055202.
[42] X. Chen, K. Liu, Z. Zhang, C. Wang, B. Li, H. Zhao, D. Zhao, D. Shen, *ACS Appl. Mater. Interfaces* **2016**, *8*, 4185.
[43] Y. Yang, W. Guo, J. Qi, J. Zhao, Y. Zhang, *Appl. Phys. Lett.* **2010**, *97*, 223113.
[44] Y. M. Juan, S. J. Chang, H. T. Hsueh, T. C. Chen, S. W. Huang, Y. H. Lee, T. J. Hsueh, C. L. Wu, *Sen. Actuators, B* **2015**, *219*, 43.
[45] Z. Bai, X. Chen, X. Yan, X. Zheng, Z. Kang, Y. Zhang, *Phys. Chem. Chem. Phys.* **2014**, *16*, 9525.
[46] X. W. Fu, Z. M. Liao, Y. B. Zhou, H. C. Wu, Y. Q. Bie, J. Xu, D. P. Yu, *Appl. Phys. Lett.* **2012**, *100*, 223114.
[47] D. Wu, Y. Jiang, Y. Zhang, Y. Yu, Z. Zhu, X. Lan, F. Li, C. Wu, L. Wang, L. Luo, *J. Mater. Chem.* **2012**, *22*, 23272.
[48] L. H. Zeng, M. Z. Wang, H. Hu, B. Nie, Y. Q. Yu, C. Y. Wu, L. Wang, J. G. Hu, C. Xie, F. X. Liang, L. B. Luo, *ACS Appl. Mater. Interfaces* **2013**, *5*, 9362.
[49] X. Li, J. Wu, N. Mao, J. Zhang, Z. Lei, Z. Liu, H. Xu, *Carbon* **2015**, *92*, 126.
[50] D. Xiang, C. Han, Z. Hu, B. Lei, Y. Liu, L. Wang, W. P. Hu, W. Chen, *Small* **2015**, *11*, 4829.
[51] X. Li, M. Zhu, M. Du, Z. Lv, L. Zhang, Y. Li, Y. Yang, T. Yang, X. Li, K. Wang, H. Zhu, Y. Fang, *Small* **2016**, *12*, 595.
[52] S. Liu, Q. Liao, S. Lu, Z. Zhang, G. Zhang, Y. Zhang, *Adv. Funct. Mater.* **2016**, *26*, 1347.
[53] W. Jin, Y. Ye, L. Gan, B. Yu, P. Wu, Y. Dai, H. Meng, X. Guo, L. Dai, *J. Mater. Chem.* **2012**, *22*, 2863.
[54] C. C. Chen, M. Aykol, C. C. Chang, A. F. J. Levi, S. B. Cronin, *Nano Lett.* **2011**, *11*, 1863.
[55] Q. Hong, Y. Cao, J. Xu, H. Lu, J. He, J. L. Sun, *ACS Appl. Mater. Interfaces* **2014**, *6*, 20887.
[56] T. Xie, M. R. Hasan, B. Qiu, E. S. Arinze, N. V. Nguyen, A. Motayed, S. M. Thon, R. Debnath, *Appl. Phys. Lett.* **2015**, *107*, 241108.
[57] Z. Chen, B. Li, X. Mo, S. Li, J. Wen, H. Lei, Z. Zhu, G. Yang, P. Gui, F. Yao, G. Fang, *Appl. Phys. Lett.* **2017**, *110*, 123504.
[58] S. Chen, X. Liu, X. Qiao, X. Wan, K. Shehzad, X. Zhang, Y. Xu, X. Fan, *Small* **2017**, *13*, 1604033.
[59] J. Zhou, L. Chen, Y. Wang, Y. He, X. Pan, E. Xie, *Nanoscale* **2016**, *8*, 50.
[60] X. Yu, Z. Zhao, J. Zhang, W. Guo, J. Qiu, D. Li, Z. Li, X. Mou, L. Li, A. Li, H. Liu, *Small* **2016**, *12*, 2759.
[61] Z. Wang, S. Ran, B. Liu, D. Chen, G. Shen, *Nanoscale* **2012**, *4*, 3350.
[62] Y. Zeng, X. Pan, W. Dai, Y. Chen, Z. Ye, *RSC Adv.* **2015**, *5*, 66738.
[63] Q. Yang, Y. Liu, Z. Li, Z. Yang, X. Wang, Z. L. Wang, *Angew. Chem., Int. Ed.* **2012**, *124*, 1.
[64] H. Lu, W. Tian, F. Cao, Y. Ma, B. Gu, L. Li, *Adv. Funct. Mater.* **2016**, *26*, 1296.
[65] S. Xu, Y. Qin, C. Xu, Y. Wei, R. Yang, Z. L. Wang, *Nat. Nanotechnol.* **2010**, *5*, 366.
[66] W. Wu, S. Bai, M. Yuan, Y. Qin, Z. L. Wang, T. Jing, *ACS Nano* **2012**, *6*, 6231.
[67] J. Xu, G. Shen, *Nano Energy* **2015**, *13*, 131.
[68] Y. Zheng, L. Cheng, M. Yuan, Z. Wang, L. Zhang, Y. Qin, T. Jing, *Nanoscale* **2014**, *6*, 7842.
[69] X. Wang, W. Song, B. Liu, G. Chen, D. Chen, C. Zhou, G. Shen, *Adv. Funct. Mater.* **2013**, *23*, 1202.
[70] H. Chen, L. F. Hu, X. S. Fang, L. M. Wu, *Adv. Funct. Mater.* **2012**, *22*,1229.

[71] Y. Hu, J. Zhou, P. H. Yeh, Z. Li, T. Y. Wei, Z. L. Wang, *Adv. Mater.* **2010**, *22*, 3327.
[72] J. Zhou, Y. Gu, Y. Hu, W. Mai, P. H. Yeh, G. Bao, A. K. Sood, D. L. Polla, Z. L. Wang, *Appl. Phys. Lett.* **2009**, *94*, 191103.
[73] T. Y. Wei, C. Te Huang, B. J. Hansen, Y. F. Lin, L. J. Chen, S. Y. Lu, Z. L. Wang, *Appl. Phys. Lett.* **2010**, *96*, 1.
[74] C. Pan, R. Yu, S. Niu, G. Zhu, Z. L. Wang, *ACS Nano* **2013**, *7*, 1803.
[75] R. Yu, C. Pan, J. Chen, G. Zhu, Z. L. Wang, *Adv. Funct. Mater.* **2013**, *23*, 5868.
[76] L. Hu, J. Yan, M. Liao, H. Xiang, X. Gong, L. Zhang, X. Fang, *Adv. Mater.* **2012**, *24*, 2305.
[77] S. M. Sze, K. K. Ng, *Physics of Semiconductor Devices*, 3rd ed., John Wiley & Sons, Inc., Hoboken, NJ **2007**.
[78] W. Zheng, T. Bian, Z. Li, M. Chen, X. Yan, Y. Dai, G. He, *J. Alloy Compd.* **2017**, *712*, 425.
[79] C. Lee, X. D. Wei, J. W. Kysar, J. Hone, *Science* **2008**, *321*, 385.
[80] Z. Zhan, L. Zheng, Y. Pan, G. Sun, L. Li, *J. Mater. Chem.* **2012**, *22*, 2589.
[81] S. Assefa, F. N. Xia, Y. A. Vlasov, *Nature* **2010**, *464*, 80.
[82] X. H. An, F. Z. Liu, Y. J. Jung, S. Kar, *Nano Lett.* **2013**, *13*, 909.
[83] P. Lv, X. Zhang, X. Zhang, W. Deng, J. Jie, *IEEE Electron Device Lett.* **2013**, *34*, 1337.
[84] E. Monroy, E. Munoz, F. J. Sanchez, F. Calle, E. Calleja, B. Beaumont, P. Gibart, J. A. Munoz, F. Cusso, *Semicond. Sci. Technol.* **1998**, *13*, 1042.
[85] E. Monroy, F. Omnes, F. Calle, *Semicond. Sci. Technol.* **2003**, *18*, R33.
[86] C. Soci, A. Zhang, X. Y. Bao, H. Kim, Y. Lo, D. Wang, *J. Nanosci. Nanotechnol.* **2010**, *10*, 1430.
[87] K. Q. Peng, S. T. Lee, *Adv. Mater.* **2011**, *23*, 198.
[88] Y. Cui, X. F. Duan, J. T. Hu, C. M. Lieber, *J. Phys. Chem. B* **2000**, *104*, 5213.
[89] E. Garnett, P. D. Yang, *Nano Lett.* **2010**, *10*, 1082.
[90] O. Gunawan, S. Guha, *Sol. Energy Mater. Sol. Cells* **2009**, *93*, 1388.
[91] B. Z. Tian, X. L. Zheng, T. J. Kempa, Y. Fang, N. F. Yu, G. H. Yu, J. L. Huang, C. M. Lieber, *Nature* **2007**, *449*, 885.
[92] T. J. Kempa, B. Z. Tian, D. R. Kim, J. S. Hu, X. L. Zheng, C. M. Lieber, *Nano Lett.* **2008**, *8*, 3456.
[93] B. Tian, T. J. Kempa, C. M. Lieber, *Chem. Soc. Rev.* **2009**, *38*, 16.
[94] J. A. Czaban, D. A. Thompson, R. R. LaPierre, *Nano Lett.* **2009**, *9*, 148.
[95] P. N. Ni, C. X. Shan, S. P. Wang, X. Y. Liu, D. Z. Shen, *J. Mater. Chem. C* **2013**, *1*, 4445.
[96] Y. H. Leung, Z. B. He, L. B. Luo, C. H. A. Tsang, N. B. Wong, W. J. Zhang, S. T. Lee, *Appl. Phys. Lett.* **2010**, *96*, 053102.
[97] G. Wang, S. Chu, N. Zhan, Y. Lin, L. Chernyak, J. Liu, *Appl. Phys. Lett.* **2011**, *98*, 041107.
[98] H. D. Cho, A. S. Zakirov, S. U. Yuldashev, C. W. Ahn, Y. K. Yeo, T. W. Kang, *Nanotechnology* **2012**, *23*, 115401.
[99] J. J. Hassan, M. A. Mahdi, S. J. Kasim, N. M. Ahmed, H. A. Hassan, Z. Hassan, *Appl. Phys. Lett.* **2012**, *101*, 261108.
[100] Y. Q. Bie, Z. M. Liao, H. Z. Zhang, G. R. Li, Y. Ye, Y. B. Zhou, J. Xu, Z. X. Qin, L. Dai, D. P. Yu, *Adv. Mater.* **2011**, *23*, 649.
[101] S. M. Hatch, J. Briscoe, S. Dunn, *Adv. Mater.* **2013**, *25*, 867.
[102] B. M. Kayes, H. A. Atwater, *J. Appl. Phys.* **2005**, *97*, 114302.
[103] T. D. Dao, C. T. T. Dang, G. HAN, C. V. Hoang, W. Yi, V. Narayanamurti, T. Nagao, *Appl. Phys. Lett.* **2013**, *103*, 193119.
[104] C. Gutsche, A. Lysov, D. Braam, I. Regolin, G. Keller, Z. A. Li, M. Geller, M. Spasova, W. Prost, F. J. Tegude, *Adv. Funct. Mater.* **2012**, *22*, 929.
[105] S. P. Mondal, S. K. Ray, *Appl. Phys. Lett.* **2009**, *94*, 223119.
[106] S. Manna, S. Das, S. P. Mondal, R. Singha, S. K. Ray, *J. Phys. Chem. C* **2012**, *116*, 7126.
[107] A. K. Katiyar, A. K. Sinha, S. Manna, R. Aluguri, S. K. Ray, *Phys. Chem. Chem. Phys.* **2013**, *15*, 20887.
[108] C. Xie, B. Nie, L. Zeng, F. X. Liang, M. Z. Wang, L. Luo, M. Feng, Y. Yu, C. Y. Wu, Y. Wu, S. H. Yu, *ACS Nano* **2014**, *8*, 4015.
[109] S. Panigrahi, D. Basak, *RSC Adv.* **2012**, *2*, 11963
[110] S. J. Hurst, E. K. Payne, L. D. Qin, C. A. Mirkin, *Angew. Chem., Int. Ed.* **2006**, *45*, 2672.
[111] D. Wang, C. M. Lieber, *Nat. Mater.* **2003**, *2*, 355.
[112] D. Wang, F. Qian, C. Yang, Z. Zhong, C. M. Lieber, *Nano Lett.* **2004**, *4*, 871.
[113] K. Sun, Y. Jing, N. Park, C. Li, Y. Bando, D. Wang, *J. Am. Chem. Soc.* **2010**, *132*, 15465.
[114] Q. Li, S. Ding, W. Zhu, L. Feng, H. Dong, W. Hu, *J. Mater. Chem. C* **2016**, *4*, 9388.
[115] H. Lin, H. Liu, X. Qian, S. W. Lai, Y. Li, N. Chen, C. Ouyang, C. M. Che, Y. Li, *Inorg. Chem.* **2011**, *50*, 7749.
[116] O. Game, U. Singh, T. Kumari, A. Banpurkar, S. Ogale, *Nanoscale* **2014**, *6*, 503.
[117] L. Zheng, P. Yu, K. Hu, F. Teng, H. Y. Chen, X. Fang, *ACS Appl. Mater. Interfaces* **2016**, *8*, 33924.
[118] Y. Dong, Y. Zou, J. Song, Z. Zhu, J. Li, H. Zeng, *Nano Energy* **2016**, *30*, 173.
[119] Y. Zhang, Y. Yu, X. Wang, G. Tong, L. Mi, Z. Zhu, X. Geng, Y. Jiang, *J. Mater. Chem. C* **2017**, *5*, 140.
[120] F. Withers, O. Del Pozo-Zamudio, A. Mishchenko, A. P. Rooney, A. Gholinia, K. Watanabe, T. Taniguchi, S. J. Haigh, A. K. Geim, A. I. Tartakovskii, K. S. Novoselov, *Nat. Mater.* **2015**, *14*, 301.
[121] N. Huo, J. Kang, Z. Wei, S. S. Li, J. Li, S. H. Wei, *Adv. Funct. Mater.* **2014**, *24*, 7025.
[122] S. Yang, C. Wang, C. Ataca, Y. Li, H. Chen, H. Cai, A. Suslu, J. C. Grossman, C. Jiang, Q. Liu, S. Tongay, *ACS Appl. Mater. Interfaces* **2016**, *8*, 2533.
[123] M. Long, E. Liu, P. Wang, A. Gao, H. Xia, W. Luo, B. Wang, J. Zeng, Y. Fu, K. Xu, W. Zhou, Y. Lv, S. Yao, M. Lu, Y. Chen, Z. Ni, Y. You, X. Zhang, S. Qin, Y. Shi, W. Hu, D. Xing, F. Miao, *Nano Lett.* **2016**, *16*, 2254.
[124] Z. L. Wang, J. H. Song, *Science* **2006**, *312*, 242.
[125] Z. L. Wang, *Mater. Sci. Eng., R* **2009**, *64*, 33.
[126] Z. L. Wang, R. S. Yang, J. Zhou, Y. Qin, C. Xu, Y. F. Hu, S. Xu, *Mater. Sci. Eng., R* **2010**, *70*, 320.
[127] Z. L. Wang, *Nano Today* **2010**, *5*, 540.
[128] X. Han, M. Chen, C. Pan, Z. L. Wang, *J. Mater. Chem. C* **2016**, *4*, 11341.
[129] S. Lu, J. Qi, S. Liu, Z. Zhang, Z. Wang, P. Lin, Q. Liao, Q. Liang, Y. Zhang, *ACS Appl. Mater. Interfaces* **2014**, *6*, 14116.
[130] Z. Zhang, Q. Liao, Y. Yu, X. Wang, Y. Zhang, *Nano Energy* **2014**, *9*, 237.
[131] P. Lin, X. Yan, Z. Zhang, Y. Shen, Y. Zhao, Z. Bai, Y. Zhang, *ACS Appl. Mater. Interfaces* **2013**, *5*, 3671.
[132] Y. Shen, X. Yan, H. Si, P. Lin, Y. Liu, Y. Sun, Y. Zhang, *ACS Appl. Mater. Interfaces* **2016**, *8*, 6137.
[133] Y. Y. Chen, C. H. Wang, G. S. Chen, Y. C. Li, C. P. Liu, *Nano Energy* **2015**, *11*, 533.
[134] S. Yan, S. C. Rai, Z. Zheng, F. Alqarni, M. Bhatt, M. A. Retana, W. Zhou, *Adv. Electron. Mater.* **2016**, *2*, 1600242.
[135] M. Peng, Y. Liu, A. Yu, Y. Zhang, C. Liu, J. Liu, W. Wu, K. Zhang, X. Shi, J. Kou, J. Zhai, Z. L. Wang, *ACS Nano* **2016**, *10*, 1572.
[136] Y. Hu, C. Pan, Z. L. Wang, *Semicond. Sci. Technol.* **2017**, *32*, 053002.
[137] Y. Xie, L. Wei, G. Wei, Q. Li, D. Wang, Y. Chen, S. Yan, G. Liu, L. Mei, J. Jiao, *Nano. Res. Lett.* **2013**, *8*, 188.
[138] W. J. Lee, M. H. Hon, *Appl. Phys. Lett.* **2011**, *99*, 251102.

[139] X. Li, C. Gao, H. Duan, B. Lu, X. Pan, E. Xie, *Nano Energy* **2012**, *1*, 640.
[140] Y. Xie, L. Wei, Q. Li, Y. Chen, S. Yan, J. Jiao, G. Liu, L. Mei, *Nanotechnology* **2014**, *25*, 075202.
[141] X. Li, C. Gao, H. Duan, B. Lu, Y. Wang, L. Chen, Z. Zhang, X. Pan, E. Xie, *Small* **2013**, *9*, 2005.
[142] Q. Zhang, G. Cao, *Nano Today* **2011**, *6*, 91.
[143] C. Gao, X. Li, Y. Wang, L. Chen, X. Pan, Z. Zhang, E. Xie, *J. Power Sources* **2013**, *239*, 458,
[144] W. Dai, X. Pan, S. Chen, C. Chen, Z. Wen, H. Zhang, Z. Ye, *J. Mater. Chem. C* **2014**, *2*, 4606.
[145] P. Guo, J. Jiang, S. Shen, L. Guo, *Int. J. Hydrogen Energy* **2013**, *38*, 13097.
[146] Y. Hu, Y. Zhang, C. Xu, G. Zhu, Z. L. Wang, *Nano Lett.* **2010**, *12*, 5025.
[147] Y. Hu, C. Xu, Y. Zhang, L. Lin, R. L. Snyder, Z. L. Wang, *Adv. Mater.* **2011**, *2*, 4068.
[148] M. Lee, J. Bae, J. Lee, C. S. Lee, S. Hong, Z. L. Wang, *Energy Environ. Sci.* **2011**, *9*, 3359.
[149] Y. Ye, L. Dai, P. C. Wu, C. Liu, T. Sun, R. M. Ma, G. G. Qin, *Nanotechnology* **2009**, *20*, 375202.
[150] C. Xu, X. D. Wang, Z. L. Wang, *J. Am. Chem. Soc.* **2009**, *131*, 5866.
[151] M. Zhou, N. Zhou, F. Kuralay, J. R. Windmiller, S. Parkhomovsky, G. Valdés, E. Katz, J. Wang, *Angew. Chem., Int. Ed.* **2012**, *51*, 2686.
[152] M. Minary-Jolandan, R. A. Bernal, I. Kuljanishvili, V. Parpoil, H. D. Espinosa, *Nano Lett.* **2012**, *12*, 970.
[153] M. N. Li, A. L. Porter, Z. L. Wang, *Nano Energy* **2017**, *34*, 93.
[154] F. R. Fan, W. Tang, Z. L. Wang, *Adv. Mater.* **2016**, *28*, 4283.
[155] S. Xu, B. J. Hansen, Z. L. Wang, *Nat. Commun.* **2010**, *1*, 93.
[156] P. Song, S. Kuang, N. Panwar, G. Yang, D. J. H. Tng, S. C. Tjin, W. J. Ng, M. B. A. Majid, G. Zhu, K. T. Yong, Z. L. Wang, *Adv. Mater.* **2017**, *29*, 1605668.
[157] H. J. Guo, T. Li, X. T. Cao, J. Xiong, Y. Jie, M. Willander, X. Cao, N. Wang, Z. L. Wang, *ACS Nano* **2017**, *11*, 856.
[158] Z. H. Lin, G. Cheng, Y. Yang, Y. S. Zhou, S. Lee, Z. L. Wang, *Adv. Funct. Mater.* **2014**, *24*, 2810.
[159] M. Zhou, J. Wang, *Electroanalysis* **2012**, *24*, 197.
[160] H. S. Jung, N. G. Park, *Small* **2015**, *11*, 10.
[161] Y. X. Zhao, K. Zhu, *Chem. Soc. Rev.* **2016**, *45*, 655.
[162] J. Chmiola, C. Largeot, P. L. Taberna, P. Simon, Y. Gogotsi, *Science* **2010**, *328*, 480.
[163] C. K. Chan, H. L. Peng, G. Liu, K. McIlwrath, X. F. Zhang, R. A. Huggins, Y. Cui, *Nat. Nanotechnol.* **2008**, *3*, 31.
[164] X. J. Hou, B. Liu, X. F. Wang, Z. R. Wang, Q. F. Wang, D. Chen, G. Z. Shen, *Nanoscale* **2013**, *5*, 7831.
[165] X. F. Wang, B. Liu, R. Liu, Q. F. Wang, X. J. Hou, D. Chen, R. M. Wang, G. Z. Shen, *Angew. Chem., Int. Ed.* **2014**, *53*, 1849.
[166] X. Wang, L. Dong, H. Zhang, R. Yu, C. Pan, Z. L. Wang, *Adv. Sci.* **2015**, *2*, 1500169.
[167] A. Chortos, J. Liu, Z. Bao, *Nat. Mater.* **2016**, *15*, 937.
[168] L. Zhang, Y. Fu, L. Xing, B. Liu, Y. Zhang, X. Xue, *J. Mater. Chem. C* **2017**, *5*, 6005.
[169] Y. Ai, Z. Lou, S. Chen, D. Chen, Z. M. Wang, K. Jiang, G. Shen, *Nano Energy* **2017**, *35*, 121.
[170] A. Carlson, A. M. Bowen, Y. G. Huang, R. G. Nuzzo, J. A. Rogers, *Adv. Mater.* **2012**, *24*, 5284.170
[171] B. Zhao, F. Wang, H. Chen, L. Zheng, L. Su, D. Zhao, X. Fang, *Adv. Funct. Mater.* **2017**, *27*, 1700264.